

Energy-momentum consistent algorithms for dynamic thermomechanical problems—Application to mortar domain decomposition problems

Christian Hesch^{*,†} and Peter Betsch

Chair of Computational Mechanics, Department of Mechanical Engineering, University of Siegen, Siegen, Germany

SUMMARY

An energy-momentum consistent integrator for non-linear thermoelastodynamics is newly developed and extended to domain decomposition problems. The energy-momentum scheme is based on the first law of thermodynamics for strongly coupled, non-linear thermoelastic problems. In contrast to staggered algorithms, a monolithic approach, which solves the mechanical as well as the thermal part simultaneously, is introduced. The approach is thermodynamically consistent in the sense that the first law of thermodynamics is fulfilled. Furthermore, a domain decomposition method for the thermoelastic system is developed based on previous developments in the context of the mortar method. The excellent performance of the new approach is illustrated in representative numerical examples. Copyright © 2011 John Wiley & Sons, Ltd.

Received 11 June 2010; Revised 25 October 2010; Accepted 1 November 2010

KEY WORDS: thermodynamics; domain decomposition; mortar method; energy momentum; coupled problems; time integration

1. INTRODUCTION

General thermoelastic material models have been a major topic in research for the past decades (see e.g. Reese and Govindjee [1] and Miehe [2] among many others). Especially the non-linear stability of the time-discrete systems has been addressed in several papers (see Simo [3]). The present paper is based on an approach by Holzapfel and Simo [4], in which rubber elasticity has been extended to a class of entropic elastic materials, written entirely in the material configuration.

Energy-momentum schemes are well known in the context of non-linear elastodynamics (see, for example, Gonzalez [5] and Betsch and Steinmann [6, 7] and the references therein) and have been applied to a wide range of applications (see e.g. for contact problems Hauret and Le Tallec [8] and Hesch and Betsch [9, 10]). They are able to conserve qualitative features of the systems and, more importantly, they exhibit an excellent performance in long-term simulations and are numerically stable. In a nutshell, in the present work we merge the concept of structure preserving integrators with the concept of entropic thermoelastic materials. In contrast to actual developments (see Romero [11, 12] and Gross [13]) we apply only a minor modification to the concept of the discrete gradient (see Gonzalez [14]), based on the first law of thermodynamics to achieve our goal.

Additionally, we introduce a structure preserving, variationally consistent mortar domain decomposition method for thermoelastic systems, based on previous developments in Hesch and Betsch

*Correspondence to: Christian Hesch, Chair of Computational Mechanics, Department of Mechanical Engineering, University of Siegen, Siegen, Germany.

†E-mail: hesch@imr.mb.uni-siegen.de

[15] confined to the isothermal case. The present domain decomposition method provides a flexible approach for the coupling of different discretization schemes or for nonmatching triangularizations. The development of variationally consistent domain decomposition constraints started two decades ago with the work of Bernadi *et al.* [16, 17]. Further advances can be found in Krause and Wohlmuth [18] and in Dohrmann *et al.* [19]. An extension to non-linear solid mechanics is given in Puso [20]. Thermomechanical contact problems using the mortar method are addressed in Hübner and Wohlmuth [21].

An outline of the present work is as follows. The fundamental equations in the context of the first law of thermodynamics are outlined in Section 2. In particular, the weak form of the balance equations is derived within this section. The equations of motion of the thermoelastic system under consideration along with the energy-momentum consistent discretization in time will be dealt with in Section 3. In Section 4 we apply a spatial discretization based on finite elements. In this connection, the use of nonconforming meshes is facilitated. Therefore, we introduce in Section 5 the mortar method for the domain decomposition of thermoelastic systems along with an energy-momentum consistent time-stepping scheme. Representative numerical examples are presented in Section 6. Eventually, conclusions are drawn in Section 7.

2. FINITE STRAIN THERMOELASTODYNAMICS

We start with a short summary of non-linear thermoelasticity. More details on the continuum description of thermoelastic solids can be found in textbooks, such as Holzapfel [22] and Gonzalez and Stuart [23]. Consider a continuum body with reference configuration $\mathcal{B}_0 \subset \mathbb{R}^3$ undergoing a motion characterized by a time-dependent deformation mapping $\varphi: \mathcal{B}_0 \times [0, T] \rightarrow \mathbb{R}^3$, where $[0, T]$ is the time interval elapsed during the motion. The current configuration is denoted by $\mathcal{B}_t = \varphi_t(\mathcal{B}_0)$. Material points are labeled by $\mathbf{X} \in \mathcal{B}_0$, the material velocity is given by $\mathbf{v}: \mathcal{B}_0 \times [0, T] \rightarrow \mathbb{R}^3$, $\mathbf{v} = \partial \varphi / \partial t$, and the deformation gradient is denoted by $\mathbf{F}: \mathcal{B}_0 \times [0, T] \rightarrow \mathbb{R}^{3 \times 3}$, $\mathbf{F} = D\varphi$. The linear momentum is given by $\boldsymbol{\pi} = \varrho_0 \mathbf{v}$, where ϱ_0 stands for the density in the reference configuration.

The absolute temperature $\theta: \mathcal{B}_0 \times [0, T] \rightarrow \mathbb{R}$ is assumed to be a smooth function of $(\mathbf{X}, t) \in \mathcal{B}_0 \times [0, T]$. We further assume that the material behavior is governed by the free energy function $\Psi: \mathcal{B}_0 \times [0, T] \rightarrow \mathbb{R}$, $\Psi = \hat{\Psi}(\mathbf{C}, \theta)$, where $\mathbf{C}: \mathcal{B}_0 \times [0, T] \rightarrow \mathbb{R}^{3 \times 3}$, $\mathbf{C} = \mathbf{F}^T \mathbf{F}$ is the right Cauchy-Green deformation tensor. Accordingly, the nominal (or first Piola-Kirchhoff) stress tensor $\mathbf{P}: \mathcal{B}_0 \times [0, T] \rightarrow \mathbb{R}^{3 \times 3}$ and the entropy $\eta: \mathcal{B}_0 \times [0, T] \rightarrow \mathbb{R}$ are defined by

$$\begin{aligned} \mathbf{P} &= 2\mathbf{F} \nabla_{\mathbf{C}} \hat{\Psi}(\mathbf{C}, \theta) \\ \eta &= -\nabla_{\theta} \hat{\Psi}(\mathbf{C}, \theta) \end{aligned} \quad (1)$$

Moreover, the nominal heat flux vector \mathbf{Q} is defined by

$$\mathbf{Q} = -\hat{\mathbf{K}}(\mathbf{C}, \theta) \text{Grad}(\theta) \quad (2)$$

Here, $\hat{\mathbf{K}}(\mathbf{C}, \theta)$ is a thermal conductivity tensor which must be positive semi-definite. Note that the constitutive laws (1) and (2) are thermodynamically consistent in the sense that they satisfy the restrictions imposed by the second law of thermodynamics (in the form of the Clausius–Duhem inequality). The Lagrangian form of the local balance of linear momentum and energy for a thermoelastic body can be written as

$$\begin{aligned} \dot{\boldsymbol{\pi}} &= \rho_0^{-1} \boldsymbol{\pi} \\ \dot{\boldsymbol{\pi}} &= \text{Div}(\mathbf{P}) + \bar{\mathbf{B}} \\ \theta \dot{\eta} &= -\text{Div}(\mathbf{Q}) + \bar{R} \end{aligned} \quad (3)$$

where $\bar{\mathbf{B}}(\mathbf{X}, t)$ and $\bar{R}(\mathbf{X}, t)$ denote the material descriptions of prescribed body force and heat supply per unit volume. The above equations have to be satisfied for all $\mathbf{X} \in \mathcal{B}_0$ and $t \geq 0$. To complete the initial-boundary value problem for the thermoelastic body under consideration, the equations

in (3) have to be supplemented by appropriate initial and boundary conditions. Accordingly, initial conditions in \mathcal{B}_0 and at time $t=0$ are specified by

$$\boldsymbol{\varphi}(\cdot, 0) = \mathbf{X}, \quad \dot{\boldsymbol{\varphi}}(\cdot, 0) = \mathbf{v}_0, \quad \theta(\cdot, 0) = \theta_0 \quad \text{in } \mathcal{B}_0 \tag{4}$$

where \mathbf{v}_0 and θ_0 are prescribed fields. Moreover, boundary conditions on $\partial\mathcal{B}_0$ at times $t \geq 0$ are specified by

$$\begin{aligned} \boldsymbol{\varphi} &= \bar{\boldsymbol{\varphi}} \quad \text{on } \partial\mathcal{B}_0^\rho \times [0, T], \quad \theta = \bar{\theta} \quad \text{on } \partial\mathcal{B}_0^\theta \times [0, T] \\ \mathbf{PN} &= \bar{\mathbf{T}} \quad \text{on } \partial\mathcal{B}_0^\sigma \times [0, T], \quad \mathbf{Q} \cdot \mathbf{N} = -\bar{\mathbf{Q}} \quad \text{on } \partial\mathcal{B}_0^Q \times [0, T] \end{aligned} \tag{5}$$

where $\partial\mathcal{B}_0^\rho$ and $\partial\mathcal{B}_0^\sigma$ are subsets of $\partial\mathcal{B}_0$ with the properties $\partial\mathcal{B}_0^\rho \cup \partial\mathcal{B}_0^\sigma = \partial\mathcal{B}_0$ and $\partial\mathcal{B}_0^\rho \cap \partial\mathcal{B}_0^\sigma = \emptyset$. Similarly, $\partial\mathcal{B}_0^\theta$ and $\partial\mathcal{B}_0^Q$ are subsets of $\partial\mathcal{B}_0$ with the properties $\partial\mathcal{B}_0^\theta \cup \partial\mathcal{B}_0^Q = \partial\mathcal{B}_0$ and $\partial\mathcal{B}_0^\theta \cap \partial\mathcal{B}_0^Q = \emptyset$. Furthermore, \mathbf{N} denotes the unit outward normal field on $\partial\mathcal{B}_0$, and $\bar{\boldsymbol{\varphi}}$, $\bar{\mathbf{T}}$, $\bar{\theta}$, and $\bar{\mathbf{Q}}$ are prescribed fields.

2.1. Weak formulation

To perform a finite element discretization in space we next recast the coupled thermoelastic problem in weak form. To this end we introduce the space of test functions \mathcal{V}_φ defined as

$$\mathcal{V}^\varphi = \{\delta\boldsymbol{\varphi}(\cdot) : \delta\boldsymbol{\varphi}(\mathbf{X}) = \mathbf{0} \text{ for } \mathbf{X} \in \partial\mathcal{B}_0^\rho\} \tag{6}$$

along with

$$\mathcal{V}^\theta = \{\delta\theta(\cdot) : \delta\theta(\mathbf{X}) = 0 \text{ for } \mathbf{X} \in \partial\mathcal{B}_0^\theta\} \tag{7}$$

Scalar multiplication of (3)₂ by the test function $\delta\boldsymbol{\varphi} \in \mathcal{V}^\varphi$ and subsequent integration yields

$$\int_{\mathcal{B}_0} \delta\boldsymbol{\varphi} \cdot \dot{\boldsymbol{\pi}} \, dV = \int_{\mathcal{B}_0} \delta\boldsymbol{\varphi} \cdot [\text{Div}(\mathbf{P}) + \bar{\mathbf{B}}] \, dV \tag{8}$$

Similarly, (3)₃ leads to

$$\int_{\mathcal{B}_0} \delta\theta\theta\dot{\eta} \, dV = \int_{\mathcal{B}_0} \delta\theta[\bar{\mathbf{R}} - \text{Div}(\mathbf{Q})] \, dV \tag{9}$$

Applying integration by parts along with the divergence theorem, (8) and (9) can be written as

$$\begin{aligned} \int_{\mathcal{B}_0} [\delta\boldsymbol{\varphi} \cdot \dot{\boldsymbol{\pi}} + D\boldsymbol{\varphi}\boldsymbol{\Sigma} : D\delta\boldsymbol{\varphi}] \, dV &= \int_{\partial\mathcal{B}_0^\sigma} \delta\boldsymbol{\varphi} \cdot \bar{\mathbf{T}} \, dA + \int_{\mathcal{B}_0} \delta\boldsymbol{\varphi} \cdot \bar{\mathbf{B}} \, dV \\ \int_{\mathcal{B}_0} [\delta\theta\theta\dot{\eta} - \mathbf{Q} \cdot \text{Grad}(\delta\theta)] \, dV &= \int_{\partial\mathcal{B}_0^Q} \delta\theta\bar{\mathbf{Q}} \, dA + \int_{\mathcal{B}_0} \delta\theta\bar{\mathbf{R}} \, dV \end{aligned} \tag{10}$$

These equations have to hold for all $\delta\boldsymbol{\varphi} \in \mathcal{V}^\varphi$ and $\delta\theta \in \mathcal{V}^\theta$. In (10)₁, the second Piola-Kirchhoff stress field $\boldsymbol{\Sigma} = D\boldsymbol{\varphi}^{-1}\mathbf{P}$ has been introduced. While the balance of linear momentum and the balance of energy are stated in weak form, we retain the kinematic relationship (3)₁ in local form.

2.2. Balance laws in global form

We next summarize fundamental balance laws in global form which should be preserved under discretization in space and time. This viewpoint leads to the notion of energy-momentum consistent integrators. The design of a specific energy-momentum consistent integrator is one of the main goals of the present work. For simplicity of exposition in what follows we restrict our attention on the thermoelastic problem with pure Neumann data, i.e. $\partial\mathcal{B}_0^\rho = \partial\mathcal{B}_0^\theta = \emptyset$. While Dirichlet boundary conditions on the mechanical part affect the momentum balance equations, Dirichlet boundary conditions on the thermal part affect the energy balance.

Setting $\delta\boldsymbol{\varphi} = \boldsymbol{\mu}$, where $\boldsymbol{\mu} \in \mathbb{R}^3$ is arbitrary and constant, showing that (10)₁ yields the balance law for *linear momentum* in integral form in a straightforward procedure:

$$\frac{d}{dt}\mathbf{L} = \int_{\partial\mathcal{B}_0^\sigma} \bar{\mathbf{T}} dA + \int_{\mathcal{B}_0} \bar{\mathbf{B}} dV \quad (11)$$

Here, the total linear momentum is given by $\mathbf{L} = \int_{\mathcal{B}_0} \boldsymbol{\pi} dV$, and the right-hand side of (11) characterizes the resultant external force applied to the continuum body.

Similarly, substituting $\delta\boldsymbol{\varphi} = \boldsymbol{\mu} \times \boldsymbol{\varphi}$ into (10)₁, the integral form of the balance law for *angular momentum* is recovered:

$$\frac{d}{dt}\mathbf{J} = \int_{\partial\mathcal{B}_0^\sigma} \boldsymbol{\varphi} \times \bar{\mathbf{T}} dA + \int_{\mathcal{B}_0} \boldsymbol{\varphi} \times \bar{\mathbf{B}} dV \quad (12)$$

In this connection, $\mathbf{J} = \int_{\mathcal{B}_0} \boldsymbol{\varphi} \times \boldsymbol{\pi} dV$ is the total angular momentum of the continuum body with respect to the origin of the inertial frame of reference. The right-hand side of (12) equals the resultant external torque about the origin.

2.2.1. Balance of energy. We next consider the integral form of the balance law for energy. As before we focus on the thermoelastic problem with pure Neumann data. Substituting $\delta\boldsymbol{\varphi} = \dot{\boldsymbol{\varphi}}$ into (10)₁ yields

$$\underbrace{\frac{d}{dt} \int_{\mathcal{B}_0} \frac{1}{2} \dot{\boldsymbol{\varphi}} \cdot \boldsymbol{\pi} dV}_{dT/dt} + \underbrace{\int_{\mathcal{B}_0} \frac{1}{2} \boldsymbol{\Sigma} : \dot{\mathbf{C}} dV}_W = \underbrace{\int_{\partial\mathcal{B}_0^\sigma} \dot{\boldsymbol{\varphi}} \cdot \bar{\mathbf{T}} dA + \int_{\mathcal{B}_0} \dot{\boldsymbol{\varphi}} \cdot \bar{\mathbf{B}} dV}_{P^{\text{ext}}} \quad (13)$$

Here, T denotes the total kinetic energy of the continuum body, W is the net working, and P^{ext} is the power of external forces. The relationship between the free energy Ψ and the specific internal energy e is given by

$$\Psi = e - \theta\eta \quad (14)$$

Differentiation with respect to time yields

$$\dot{\Psi} = \dot{e} - \dot{\theta}\eta - \theta\dot{\eta} \quad (15)$$

On the other hand the constitutive Equations (1) are based on the free energy function $\Psi = \hat{\Psi}(\mathbf{C}, \theta)$, and thus imply

$$\dot{\Psi} = \underbrace{\frac{\partial \hat{\Psi}(\mathbf{C}, \theta)}{\partial \mathbf{C}}}_{\frac{1}{2}\boldsymbol{\Sigma}} : \dot{\mathbf{C}} + \underbrace{\frac{\partial \hat{\Psi}(\mathbf{C}, \theta)}{\partial \theta}}_{-\eta} \dot{\theta} \quad (16)$$

Accordingly, taking into account (15) and (16), the stress power can be written as

$$\frac{1}{2}\boldsymbol{\Sigma} : \dot{\mathbf{C}} = \dot{e} - \theta\dot{\eta} \quad (17)$$

Introducing the total internal energy of the continuum body $E = \int_{\mathcal{B}_0} e dV$, the net working can now be written in the form

$$W = \dot{E} - \int_{\mathcal{B}_0} \theta\dot{\eta} dV \quad (18)$$

Testing (10)₂ on the constant $\delta\boldsymbol{\varphi} = \boldsymbol{\mu}$, $\boldsymbol{\mu} \in \mathbb{R}$, gives

$$\int_{\mathcal{B}_0} \theta\dot{\eta} dV = - \int_{\partial\mathcal{B}_0} \mathbf{Q} \cdot \mathbf{N} dA + \int_{\mathcal{B}_0} \bar{\mathbf{R}} dV =: Q \quad (19)$$

where Q is the total net heating of the continuum body. Substituting (19) into (18), we recover the first law of thermodynamics in the form $dE/dt = W + Q$. Moreover, in view of (13), the global form of the energy balance law can be written as

$$\frac{d}{dt}[T + E] = P^{ext} + Q \tag{20}$$

In case the external forces are associated with a potential energy V^{ext} , i.e. $P^{ext} = -dV^{ext}/dt$, the energy balance law reads as

$$\frac{d}{dt}[T + E + V^{ext}] = Q \tag{21}$$

Concerning the discretization in space and time of the coupled thermoelastic problem under consideration we aim at numerical methods that correctly reproduce the above balance laws for any time step. For example, if the external forces vanish the linear momentum as well as the angular momentum of the system should be conserved exactly. Moreover, if (21) applies and the system is insulated (i.e. $Q=0$), the total energy should be exactly conserved in the discrete setting thus correctly reproducing the continuous law (21).

3. DISCRETIZATION IN TIME

We next perform the discretization in time of the coupled thermoelastic problem under consideration. In particular, we present a new energy-momentum consistent integrator for thermoelastodynamics.

Consider a sequence of times $t_0, \dots, t_n, t_{n+1}, \dots$ and assume that the state at t_n , denoted by (φ_n, θ_n) , is known. Then the goal is to approximate the state $(\varphi_{n+1}, \theta_{n+1})$ at t_{n+1} , where the time-step size $\Delta t = t_{n+1} - t_n$ is prescribed. Consider the algorithmic approximation to the weak form (10) defined by

$$\begin{aligned} \int_{\mathcal{B}_0} \left[\delta \varphi \cdot \frac{\pi_{n+1} - \pi_n}{\Delta t} + D \varphi_{n+1/2} \Sigma_{n,n+1} : D \delta \varphi \right] dV &= \int_{\partial \mathcal{B}_0^\sigma} \delta \varphi \cdot \bar{T}_{n+1/2} dA + \int_{\mathcal{B}_0} \delta \varphi \cdot \bar{B}_{n+1/2} dV \\ \int_{\mathcal{B}_0} \left[\delta \theta \theta_{n+1/2} \frac{\eta_{n+1} - \eta_n}{\Delta t} - Q_{n,n+1} \cdot \text{Grad}(\delta \theta) \right] dV &= \int_{\partial \mathcal{B}_0^Q} \delta \theta \bar{Q}_{n+1/2} dA + \int_{\mathcal{B}_0} \delta \theta \bar{R}_{n+1/2} dV \end{aligned} \tag{22}$$

The above two equations are supplemented by the mid-point-type approximation to the kinematic relationship (3)₁ given by

$$\varphi_{n+1} - \varphi_n = \Delta t v_{n+1/2} \tag{23}$$

together with

$$\pi_{n+\alpha} = \varrho_0 v_{n+\alpha} \quad \text{for } \alpha \in \{0, \frac{1}{2}, 1\} \tag{24}$$

In the above formulas, $(\cdot)_{n+1/2}$ denotes the standard mid-point approximation, e.g. $\varphi_{n+1/2} = \frac{1}{2}(\varphi_{n+1} + \varphi_n)$. Moreover, in (22)₁, $\Sigma_{n,n+1}$ denotes a consistent algorithmic version of the second Piola-Kirchhoff stress tensor defined by

$$\Sigma_{n,n+1} = \nabla_C \hat{\Psi}(C_{n+1/2}, \theta_{n+1/2}) + \frac{e_{n+1} - e_n - \theta_{n+1/2} \Delta \eta - \nabla_C \hat{\Psi}(C_{n+1/2}, \theta_{n+1/2}) : \Delta C}{\Delta C : \Delta C} \Delta C \tag{25}$$

where

$$\begin{aligned} C_{n+1/2} &= \frac{1}{2}(C_n + C_{n+1}) \\ \Delta C &= C_{n+1} - C_n, \quad \Delta \eta = \eta_{n+1} - \eta_n \end{aligned} \tag{26}$$

In this connection, (14) gives rise to

$$e_k = \hat{\Psi}(\mathbf{C}_k, \theta_k) - \theta_k \nabla_{\theta} \hat{\Psi}(\mathbf{C}_k, \theta_k) \quad (27)$$

for $k \in \{n, n+1\}$. Accordingly, the algorithmic stress $\Sigma_{n,n+1}$ just depends on the state variables $(\boldsymbol{\varphi}_n, \theta_n)$ and $(\boldsymbol{\varphi}_{n+1}, \theta_{n+1})$. We further remark that in the isothermal limit formula (25) boils down to the discrete gradient in the sense of Gonzalez [14] corresponding to $De(\mathbf{C})$, see also Gonzalez [5] and Betsch and Steinmann [6].

In $(22)_2$, $\mathbf{Q}_{n,n+1}$ denotes a consistent algorithmic version of the nominal heat flux vector defined by

$$\mathbf{Q}_{n,n+1} = -\widehat{\mathbf{K}}(\mathbf{C}_{n+1/2}, \theta_{n+1/2}) \text{Grad}(\theta_{n+1/2}) \quad (28)$$

3.1. Algorithmic versions of the global balance laws

We next verify that the newly proposed energy-momentum consistent integrator does indeed satisfy the global balance laws summarized in Section 2.2. Again we focus on pure Neumann data. Inserting $\delta\boldsymbol{\varphi} = \boldsymbol{\mu}$ into $(22)_1$ yields

$$\mathbf{L}_{n+1} - \mathbf{L}_n = \Delta t \int_{\partial\mathcal{B}_0^{\sigma}} \bar{\mathbf{T}}_{n+1/2} dA + \int_{\mathcal{B}_0} \bar{\mathbf{B}}_{n+1/2} dV \quad (29)$$

Furthermore, inserting $\delta\boldsymbol{\varphi} = \boldsymbol{\mu} \times \boldsymbol{\varphi}_{n+1/2}$ into $(22)_1$ yields

$$\mathbf{J}_{n+1} - \mathbf{J}_n = \Delta t \int_{\partial\mathcal{B}_0^{\sigma}} \boldsymbol{\varphi}_{n+1/2} \times \bar{\mathbf{T}}_{n+1/2} dA + \int_{\mathcal{B}_0} \boldsymbol{\varphi}_{n+1/2} \times \bar{\mathbf{B}}_{n+1/2} dV \quad (30)$$

The last two results can be viewed as time-discrete counterparts of the global balance laws for linear and angular momentum. To show algorithmic satisfaction of the global balance law for energy, substitute $\mathbf{v}_{n+1/2}$ for $\delta\boldsymbol{\varphi}$ in $(22)_1$ to obtain

$$\int_{\mathcal{B}_0} [\varrho_0 \mathbf{v}_{n+1/2} \cdot (\mathbf{v}_{n+1} - \mathbf{v}_n) + D\boldsymbol{\varphi}_{n+1/2} \Sigma_{n,n+1} : (D\boldsymbol{\varphi}_{n+1} - D\boldsymbol{\varphi}_n)] dV = \Delta t P_{n,n+1}^{\text{ext}} \quad (31)$$

where use has been made of (23). On the right-hand side of the last equation $P_{n,n+1}^{\text{ext}}$ stands for the algorithmic version of the power of external forces given by

$$P_{n,n+1}^{\text{ext}} = \int_{\partial\mathcal{B}_0^{\sigma}} \mathbf{v}_{n+1/2} \cdot \bar{\mathbf{T}} dA + \int_{\mathcal{B}_0} \mathbf{v}_{n+1/2} \cdot \bar{\mathbf{B}} dV \quad (32)$$

Taking into account the symmetry of $\Sigma_{n,n+1}$ along with the definition of the kinetic energy, (31) can be recast in the form

$$T_{n+1} - T_n + \int_{\mathcal{B}_0} \frac{1}{2} \Sigma_{n,n+1} : (\mathbf{C}_{n+1} - \mathbf{C}_n) dV = \Delta t P_{n,n+1}^{\text{ext}} \quad (33)$$

In view of the definition of the algorithmic stress tensor (25), the last equation can be written as

$$T_{n+1} - T_n + E_{n+1} - E_n - \int_{\mathcal{B}_0} \theta_{n+1/2} (\eta_{n+1} - \eta_n) dV = \Delta t P_{n,n+1}^{\text{ext}} \quad (34)$$

Now, setting $\delta\theta = \mu$ in $(22)_2$ yields

$$\frac{1}{\Delta t} \int_{\mathcal{B}_0} \theta_{n+1/2} (\eta_{n+1} - \eta_n) dV = - \int_{\partial\mathcal{B}_0} \mathbf{Q}_{n,n+1} \cdot \mathbf{N} dA + \int_{\mathcal{B}_0} \bar{\mathbf{R}}_{n+1/2} dV =: Q_{n,n+1} \quad (35)$$

Here, $Q_{n,n+1}$ denotes the discrete version of the total net heating. Combining (34) and (35) we arrive at the result

$$T_{n+1} - T_n + E_{n+1} - E_n = \Delta t [P_{n,n+1}^{\text{ext}} + Q_{n,n+1}] \quad (36)$$

The last equation confirms algorithmic energy consistency of the integrator under consideration. That is, the balance law for energy (20) is correctly reproduced in the discrete setting for any time-step size Δt .

4. DISCRETIZATION IN SPACE

To achieve a numerical solution for the semi-discrete, coupled thermoelastic problem, we apply a finite element framework to both, the mechanical as well as the thermal field. In particular, we consider a standard displacement-based finite element approach, where we introduce finite dimensional approximations of $\boldsymbol{\varphi}$ and $\delta\boldsymbol{\varphi}$ so that

$$\boldsymbol{\varphi}^h = \sum_{A \in \omega} N^A(\mathbf{X})\mathbf{q}_A \quad \text{and} \quad \delta\boldsymbol{\varphi}^h = \sum_{B \in \omega} N^B(\mathbf{X})\delta\mathbf{q}_B \tag{37}$$

Here, $A \in \omega = \{1, \dots, n_{\text{node}}\}$ such that $\mathbf{q}_A \in \mathbb{R}^3$ denotes the position vector of node A and $N^A(\mathbf{X}): \mathcal{B}_0 \rightarrow \mathbb{R}$ are global shape functions. In the present work, we make use of standard trilinear shape functions. In a second step, we discretize the temperature field using the same shape functions as before

$$\theta^h = \sum_{A \in \omega} N^A(\mathbf{X})\Theta_A \quad \text{and} \quad \delta\theta^h = \sum_{B \in \omega} N^B(\mathbf{X})\delta\Theta_B \tag{38}$$

where $\Theta_A \in \mathbb{R}$ denotes the temperature at node $A \in \omega = \{1, \dots, n_{\text{node}}\}$. For later use we introduce the system vectors $\mathbf{q} = [\mathbf{q}_1, \dots, \mathbf{q}_{n_{\text{node}}}]$, $\boldsymbol{\Theta} = [\Theta_1, \dots, \Theta_{n_{\text{node}}}]$ and the variations thereof as $\delta\mathbf{q} = [\delta\mathbf{q}_1, \dots, \delta\mathbf{q}_{n_{\text{node}}}]$ and $\delta\boldsymbol{\Theta} = [\delta\Theta_1, \dots, \delta\Theta_{n_{\text{node}}}]$.

Next we develop the fully discretized weak form based on the semi-discrete formulation (22), starting with the first term in (22)₁

$$\begin{aligned} \int_{\mathcal{B}_0} \delta\boldsymbol{\varphi}^h \cdot \frac{\boldsymbol{\pi}_{n+1}^h - \boldsymbol{\pi}_n^h}{\Delta t} dV &= \frac{1}{\Delta t} \delta\mathbf{q}_A \cdot \int_{\mathcal{B}_0} \rho_0 N^A N^B dV (\mathbf{v}_{B,n+1} - \mathbf{v}_{B,n}) \\ &= \frac{1}{\Delta t} \delta\mathbf{q}_A \cdot \mathbf{M}^{AB} (\mathbf{v}_{B,n+1} - \mathbf{v}_{B,n}) \end{aligned} \tag{39}$$

where (23) and (24) have been taken into account. For simplicity of exposition we make use of the summation convention for repeated indices. Similarly, we obtain for the first term in (22)₂

$$\begin{aligned} \int_{\mathcal{B}_0} \delta\theta^h \theta_{n+1/2}^h \frac{\eta_{n+1}^h - \eta_n^h}{\Delta t} dV &= \frac{1}{\Delta t} \delta\Theta_A \int_{\mathcal{B}_0} (\eta_{n+1}^h - \eta_n^h) N^A N^B dV \Theta_{B,n+1/2} \\ &= \frac{1}{\Delta t} \delta\Theta_A \Gamma_{n,n+1}^{AB} \Theta_{B,n+1/2} \end{aligned} \tag{40}$$

where, in view of (1)₂, the discrete entropy reads as

$$\eta_k^h = \nabla_{\theta} \Psi(\mathbf{C}_k^h, \theta_k^h), \quad k \in \{n, n+1\} \tag{41}$$

and the discrete right Cauchy-Green tensor is given by

$$\mathbf{C}_k^h = (D\boldsymbol{\varphi}_k^h)^T D\boldsymbol{\varphi}_k^h, \quad k \in \{n, n+1\} \tag{42}$$

Next we approximate the second term in (22)₁ as follows:

$$\begin{aligned} \int_{\mathcal{B}_0} D\boldsymbol{\varphi}_{n+1/2}^h \cdot \boldsymbol{\Sigma}_{n,n+1}^h : D\delta\boldsymbol{\varphi}^h dV &= \delta\mathbf{q}_A \cdot \int_{\mathcal{B}_0} \nabla N^A \cdot \boldsymbol{\Sigma}_{n,n+1}^h \nabla N^B dV \mathbf{q}_{B,n+1/2} \\ &= \delta\mathbf{q}_A \cdot \int_{\mathcal{B}_0} \mathbf{S}_{n,n+1}^{AB} dV \mathbf{q}_{B,n+1/2} \end{aligned} \tag{43}$$

Analogue to (25), $\Sigma_{n,n+1}^h$ denotes a consistent algorithmic version of the discrete second Piola-Kirchhoff stress tensor, defined by

$$\Sigma_{n,n+1}^h = \nabla_C \Psi(\mathbf{C}_{n+1/2}^h, \theta_{n+1/2}^h) + \frac{e_{n+1}^h - e_n^h - \theta_{n+1/2}^h \Delta \eta^h - \nabla_C \Psi(\mathbf{C}_{n+1/2}^h, \theta_{n+1/2}^h) : \Delta \mathbf{C}^h}{\Delta \mathbf{C}^h : \Delta \mathbf{C}^h} \Delta \mathbf{C}^h \quad (44)$$

As before, we formulate the inner energy in terms of the free Helmholtz energy

$$e_k = \Psi(\mathbf{C}_k^h, \theta_k^h) - \theta_k^h \nabla_\theta \Psi(\mathbf{C}_k^h, \theta_k^h), \quad k \in \{n, n+1\} \quad (45)$$

Similarly, the second term in (22)₂ yields

$$\begin{aligned} \int_{\mathcal{B}_0} \text{Grad}(\delta \theta^h) \cdot \mathbf{Q}_{n,n+1}^h \, dV &= -\delta \Theta_A \int_{\mathcal{B}_0} \nabla N^A \cdot \widehat{\mathbf{K}}(\mathbf{C}_{n+1/2}^h, \theta_{n+1/2}^h) \nabla N^B \, dV \Theta_{B,n+1/2} \\ &= -\delta \Theta_A \int_{\mathcal{B}_0} K_{n,n+1}^{AB} \, dV \Theta_{B,n+1/2} \end{aligned} \quad (46)$$

At last, the terms on the right side of (22)₁ and (22)₂ can be written as

$$\begin{aligned} \int_{\partial \mathcal{B}_0^T} \delta \boldsymbol{\varphi}^h \cdot \bar{\mathbf{T}}_{n+1/2} \, dA + \int_{\mathcal{B}_0} \delta \boldsymbol{\varphi}^h \cdot \bar{\mathbf{B}}_{n+1/2} \, dV &= \delta \mathbf{q}_A \cdot \left[\int_{\partial \mathcal{B}_0^T} N^A \bar{\mathbf{T}}_{n+1/2} \, dA + \int_{\mathcal{B}_0} N^A \bar{\mathbf{B}}_{n+1/2} \, dV \right] \\ &= \delta \mathbf{q}_A \cdot \mathbf{F}_{n+1/2}^{A, \text{ext}} \\ \int_{\partial \mathcal{B}_0^Q} \delta \theta^h \bar{\mathbf{Q}}_{n+1/2} \, dA + \int_{\mathcal{B}_0} \delta \theta^h \bar{\mathbf{R}}_{n+1/2} \, dV &= \delta \Theta_A \left[\int_{\partial \mathcal{B}_0^Q} N^A \bar{\mathbf{Q}}_{n+1/2} \, dA + \int_{\mathcal{B}_0} N^A \bar{\mathbf{R}}_{n+1/2} \, dV \right] \\ &= \delta \Theta_A \mathbf{Q}_{n,n+1}^{h,A} \end{aligned} \quad (47)$$

which completes the spatial discretization process. In summary, we receive the following equations:

$$\begin{aligned} \delta \mathbf{q}_A \cdot \left[M^{AB} (\mathbf{v}_{B,n+1} - \mathbf{v}_{B,n}) + \Delta t \int_{\mathcal{B}_0} S_{n,n+1}^{AB} \, dV \mathbf{q}_{B,n+1/2} \right] &= \Delta t \delta \mathbf{q}_A \cdot [\mathbf{F}_{n+1/2}^{A, \text{ext}}] \\ \delta \Theta_A \left[\Gamma_{n,n+1}^{AB} \Theta_{B,n+1/2} - \Delta t \int_{\mathcal{B}_0} K_{n,n+1}^{AB} \, dV \Theta_{B,n+1/2} \right] &= \Delta t \delta \Theta_A \mathbf{Q}_{n,n+1}^{h,A} \end{aligned} \quad (48)$$

Next, we verify that the spatial discretization of the coupled thermoelastic system inherits the fundamental conservation properties of the underlying semi-discrete system.

4.1. Conservation properties

4.1.1. *Linear momentum.* To verify conservation of linear momentum, we focus again on pure Neumann data. Insertion of $\delta \mathbf{q}^A = \boldsymbol{\mu}$ into (48)₁ and summation yields

$$\boldsymbol{\mu} \cdot (\mathbf{L}_{n+1} - \mathbf{L}_n) = \Delta t \sum_{A \in \omega} \boldsymbol{\mu} \cdot \left[- \int_{\mathcal{B}_0} S_{n,n+1}^{AB} \, dV \mathbf{q}_{B,n+1/2} + \mathbf{F}_{n+1/2}^{A, \text{ext}} \right] \quad (49)$$

With regard to (43) we can state

$$\boldsymbol{\mu} \cdot \int_{\mathcal{B}_0} \left(\nabla \sum_{A \in \omega} N^A \right) \cdot \Sigma_{n,n+1}^h \nabla N^B \, dV \mathbf{q}_{B,n+1/2} = 0 \quad (50)$$

and obtain for the discrete counterpart of (29)

$$\mathbf{L}_{n+1} - \mathbf{L}_n = \Delta t \sum_{A \in \omega} \mathbf{F}_{n+1/2}^{A, \text{ext}} \quad (51)$$

4.1.2. *Angular momentum.* Next, we substitute $\delta \mathbf{q}_A = \boldsymbol{\mu} \times \mathbf{q}_{A,n+1/2}$ into (48)₁ and obtain

$$\boldsymbol{\mu} \cdot (\mathbf{J}_{n+1} - \mathbf{J}_n) = \Delta t \boldsymbol{\mu} \cdot \sum_{A \in \omega} \mathbf{q}_{A,n+1/2} \times \left[- \int_{\mathcal{B}_0} S_{n,n+1}^{AB} dV \mathbf{q}_{B,n+1/2} + \mathbf{F}_{n+1/2}^{A,ext} \right] \quad (52)$$

Due to the skew-symmetry of $\mathbf{q}_{A,n+1/2} \times \mathbf{q}_{B,n+1/2}$ and the symmetry of $S_{n,n+1}^{AB}$ we obtain the discrete counterpart of (30)

$$\mathbf{J}_{n+1} - \mathbf{J}_n = \Delta t \sum_{A \in \omega} \mathbf{q}_{A,n+1/2} \times \mathbf{F}_{n+1/2}^{A,ext} \quad (53)$$

4.1.3. *Total energy.* Eventually, we verify algorithmic conservation of energy. Replacing $\delta \mathbf{q}_A$ in (48)₁ with $\mathbf{v}_{A,n+1/2}$ and summation over all nodes yields

$$T_{n+1} - T_n + \int_{\mathcal{B}_0} \sum_{A \in \omega} [(\mathbf{q}_{A,n+1} - \mathbf{q}_{A,n}) \cdot S_{n,n+1}^{AB} \mathbf{q}_{B,n+1/2}] dV = \Delta t \mathbf{v}_{A,n+1/2} \cdot \mathbf{F}_{n+1/2}^{A,ext} \quad (54)$$

With regard to (43) one can rewrite the last equation as

$$T_{n+1} - T_n + \int_{\mathcal{B}_0} \boldsymbol{\Sigma}_{n,n+1}^h : (\mathbf{C}_{n+1}^h - \mathbf{C}_n^h) dV = \Delta t P_{n,n+1}^{h,ext} \quad (55)$$

Taking (44) into account, we obtain

$$T_{n+1} - T_n + \int_{\mathcal{B}_0} [e_{n+1}^h - e_n^h - \theta_{n+1/2}^h (\eta_{n+1}^h - \eta_n^h)] dV = \Delta t P_{n,n+1}^{h,ext} \quad (56)$$

In a second step we set $\delta \theta_A = \mu$ and obtain from (48)₂

$$\int_{\mathcal{B}_0} \left[\theta_{n+1/2}^h (\eta_{n+1}^h - \eta_n^h) - \Delta t \left(\nabla \sum_{A \in \omega} N^A \right) \cdot \mathbf{K}^h(\mathbf{C}_{n+1/2}^h, \theta_{n+1/2}^h) \nabla N^B \Theta_{B,n+1/2} \right] dV = \Delta t Q_{n,n+1}^h \quad (57)$$

Thus, we arrive at

$$T_{n+1} - T_n + E_{n+1} - E_n = \Delta t [P_{n,n+1}^{h,ext} + Q_{n,n+1}^h] \quad (58)$$

which proves algorithmic energy consistency.

5. FOUR-DIMENSIONAL MORTAR METHOD

The goal of this section is to extend our previous developments to domain decomposition problems in dynamic thermoelasticity. In what follows, we focus on specific coupling terms in the weak form arising from the tying of dissimilarly meshed regions using quadrilateral meshes. Note, however, that the presented segmentation process can be easily applied to other meshes as well.

Consider a body subdivided into two parts as depicted in Figure 1. The two parts are tied together at a common interface Γ_d . While the weak form corresponding to each subdomain $\mathcal{B}_0^{(i)}, i \in \{1, 2\}$,

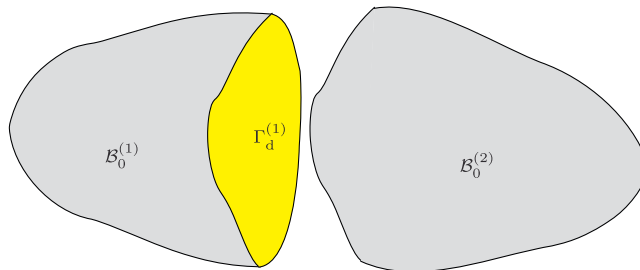


Figure 1. Decomposition of a body into two domains with the internal interface Γ_d .

is again given by (10), the coupling of both subdomains gives rise to the additional interface contributions

$$G^d = \int_{\Gamma_d^{(1)}} \boldsymbol{t}^{(1)} \cdot \left(\begin{bmatrix} \delta \boldsymbol{\varphi}^{(1)} \\ \delta \theta^{(1)} \end{bmatrix} - \begin{bmatrix} \delta \boldsymbol{\varphi}^{(2)} \\ \delta \theta^{(2)} \end{bmatrix} \right) d\Gamma \quad (59)$$

The quantity $\boldsymbol{t}^{(1)} \in \mathbb{R}^4$ will later on denote the Lagrange multipliers, which can be interpreted as Piola tractions for the mechanical part and have the dimension of the entropy for the thermal part. Applying the mortar method, we discretize $\boldsymbol{t}^{(1)}$ using the shape functions of the underlying geometry, i.e.

$$\boldsymbol{t}^{(1),h} = \sum_{A \in \bar{\omega}^{(1)}} N^A(\boldsymbol{X}^{(1)}) \boldsymbol{\lambda}_A \quad (60)$$

where $\bar{\omega}^{(1)} = [1, \dots, n_{\text{surf}}]$ denotes the set of nodes on the internal interfaces $\Gamma_d^{(1)}$. Insertion of the approximations (37), (38) and (60) in (59) yields

$$\begin{aligned} G^d(\delta \boldsymbol{q}, \delta \boldsymbol{\Theta}, \boldsymbol{\lambda}) &= \int_{\Gamma_d^{(1)}} \boldsymbol{t}^{(1),h} \cdot \left(\begin{bmatrix} \delta \boldsymbol{\varphi}^{(1),h} \\ \delta \theta^{(1),h} \end{bmatrix} - \begin{bmatrix} \delta \boldsymbol{\varphi}^{(2),h} \\ \delta \theta^{(2),h} \end{bmatrix} \right) d\Gamma \\ &= \sum_{A \in \bar{\omega}^{(1)}} \boldsymbol{\lambda}_A \cdot \left(\sum_{B \in \bar{\omega}^{(1)}} n^{AB} \begin{bmatrix} \delta \boldsymbol{q}_B^{(1)} \\ \delta \boldsymbol{\Theta}_B^{(1)} \end{bmatrix} - \sum_{C \in \bar{\omega}^{(2)}} n^{AC} \begin{bmatrix} \delta \boldsymbol{q}_C^{(2)} \\ \delta \boldsymbol{\Theta}_C^{(2)} \end{bmatrix} \right) \end{aligned} \quad (61)$$

where n^{AB} and n^{AC} denote the so-called mortar integrals given by

$$\begin{aligned} n^{AB} &= \int_{\Gamma_d^{(1)}} N^A(\boldsymbol{X}^{(1)}) N^B(\boldsymbol{X}^{(1)}) d\Gamma \\ n^{AC} &= \int_{\Gamma_d^{(1)}} N^A(\boldsymbol{X}^{(1)}) N^C(\boldsymbol{X}^{(2)}) d\Gamma \end{aligned} \quad (62)$$

The nodal Lagrange multipliers $\boldsymbol{\lambda}_A \in \mathbb{R}^4$ characterize the generalized forces of constraint for enforcing the mortar mesh-tying constraint, given by

$$\boldsymbol{\Phi}_{\text{mortar}}^A(\boldsymbol{q}, \boldsymbol{\Theta}) = n^{AB} \begin{bmatrix} \boldsymbol{q}_B^{(1)} \\ \boldsymbol{\Theta}_B^{(1)} \end{bmatrix} - n^{AC} \begin{bmatrix} \boldsymbol{q}_C^{(2)} \\ \boldsymbol{\Theta}_C^{(2)} \end{bmatrix} \quad (63)$$

To evaluate the mortar integrals, we have to divide both sides of the discrete interface into segments. We will summarize this process in the following, for further details see Puso [20] and Hesch and Betsch [15].

5.1. Segmentation

We consider a typical element $e_2 \in \bar{e}^{(2)}$, where $\bar{e}^{(2)}$ denotes the set of elements on the discrete surface $\Gamma_d^{(2),h}$ of an arbitrarily chosen side (2), referred to as mortar side, with the nodes $\boldsymbol{q}_1^{(2)}$, $\boldsymbol{q}_2^{(2)}$, $\boldsymbol{q}_3^{(2)}$, and $\boldsymbol{q}_4^{(2)}$ of the element e_2 . These nodes are projected orthogonally to the opposing non-mortar side $\Gamma_d^{(1),h}$. Each orthogonally projected node I can be written in terms of convective coordinates $\bar{\boldsymbol{\xi}}_I^{(1)}$ (see Figure 2(b)) of the opposing elements, which are collected in a vector

$$\bar{\boldsymbol{\xi}}^{(1)} = [\bar{\boldsymbol{\xi}}_1^{(1)}, \bar{\boldsymbol{\xi}}_2^{(1)}, \bar{\boldsymbol{\xi}}_3^{(1)}, \bar{\boldsymbol{\xi}}_4^{(1)}] \quad (64)$$

Next a clipping algorithm is used to determine the segments, corresponding to each pair of elements $e \in \bar{e}^{(1)}$ and e_2 , where $\bar{e}^{(1)}$ denotes the set of elements on the interface $\Gamma_d^{(1),h}$. Each specific segment depends on the corresponding nodal coordinates which can be collected in the ordered set

$$\eta^{\text{seg}} = \{\boldsymbol{q}_{1-4}^{(1)}, \boldsymbol{q}_{1-4}^{(2)}\} \quad (65)$$

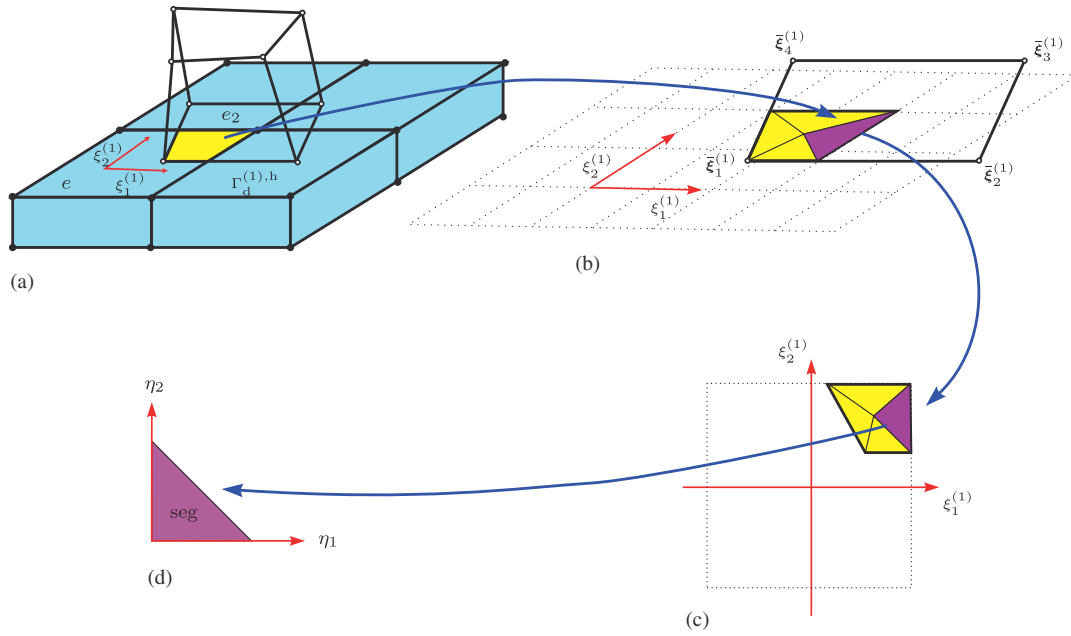


Figure 2. Segmentation process: (a) Representative element e on the non-mortar side $\Gamma_d^{(1),h}$ and one opposing element e_2 on the mortar side; (b) Projection of the nodal points of element e_2 onto the non-mortar side and determination of the relevant segments; (c) Location of the segments in the $\xi_1^{(1)}, \xi_2^{(1)}$ coordinate system; and (d) Coordinate transformation of each segment to a reference triangle with coordinates η_1, η_2 .

relevant to the segment at hand. For each segment a linear transformation $\boldsymbol{\eta} \rightarrow \boldsymbol{\xi}_{\text{seg}}^{(i),h}$ of the form (see Figures 2(c) and (d))

$$\boldsymbol{\xi}_{\text{seg}}^{(i),h}(\boldsymbol{\eta}) = \sum_{K=1}^3 M^K(\boldsymbol{\eta}) \boldsymbol{\xi}_{\text{seg},K}^{(i)}, \quad i \in \{1, 2\} \tag{66}$$

is introduced, where $\boldsymbol{\xi}_{\text{seg},K}^{(i)}$ denotes the vertices of the segment. In accordance with the results of the clipping algorithm, linear triangular shape functions M^K are used. Now we obtain for the discrete values on the interface

$$\boldsymbol{t}_{\text{seg}}^{(1),h} = \sum_{\kappa} N^{\kappa}(\boldsymbol{\xi}_{\text{seg}}^{(1),h}(\boldsymbol{\eta})) \boldsymbol{\lambda}_{\kappa} \tag{67}$$

$$\boldsymbol{\varphi}_{\text{seg}}^{(1),h} = \sum_{\beta} N^{\beta}(\boldsymbol{\xi}_{\text{seg}}^{(1),h}(\boldsymbol{\eta})) \boldsymbol{q}_{\beta}^{(1)}, \quad \boldsymbol{\varphi}_{\text{seg}}^{(2),h} = \sum_{\zeta} N^{\zeta}(\boldsymbol{\xi}_{\text{seg}}^{(2),h}(\boldsymbol{\eta})) \boldsymbol{q}_{\zeta}^{(2)} \tag{68}$$

$$\boldsymbol{\theta}_{\text{seg}}^{(1),h} = \sum_{\beta} N^{\beta}(\boldsymbol{\xi}_{\text{seg}}^{(1),h}(\boldsymbol{\eta})) \boldsymbol{\Theta}_{\beta}^{(1)}, \quad \boldsymbol{\theta}_{\text{seg}}^{(2),h} = \sum_{\zeta} N^{\zeta}(\boldsymbol{\xi}_{\text{seg}}^{(2),h}(\boldsymbol{\eta})) \boldsymbol{\Theta}_{\zeta}^{(2)} \tag{69}$$

Here, κ, β , and ζ denote the nodes corresponding to each particular segment. The mortar integrals for each segment can now be calculated as follows:

$$n^{\kappa\beta} = \int_{\Gamma_{d,\text{seg}}^{(1)}} N^{\kappa}(\boldsymbol{\xi}_{\text{seg}}^{(1),h}(\boldsymbol{\eta})) N^{\beta}(\boldsymbol{\xi}_{\text{seg}}^{(1),h}(\boldsymbol{\eta})) d\Gamma \tag{70}$$

$$n^{\kappa\zeta} = \int_{\Gamma_{d,\text{seg}}^{(1)}} N^{\kappa}(\boldsymbol{\xi}_{\text{seg}}^{(1),h}(\boldsymbol{\eta})) N^{\zeta}(\boldsymbol{\xi}_{\text{seg}}^{(2),h}(\boldsymbol{\eta})) d\Gamma$$

Furthermore, the Jacobian J_{seg} is required

$$J_{\text{seg}} = \|\boldsymbol{A}_1(\boldsymbol{\xi}_{\text{seg}}^{(1),h}(\boldsymbol{\eta})) \times \boldsymbol{A}_2(\boldsymbol{\xi}_{\text{seg}}^{(2),h}(\boldsymbol{\eta}))\| \det(D\boldsymbol{\xi}(\boldsymbol{\eta})) \tag{71}$$

where we have made use of the convective base vectors

$$\mathbf{A}_\alpha(\boldsymbol{\xi}_{\text{seg}}^{(1),h}(\boldsymbol{\eta})) = \sum_{\kappa} N_{,\alpha}^{\kappa}(\boldsymbol{\xi}_{\text{seg}}^{(1),h}(\boldsymbol{\eta})) \mathbf{X}_{\kappa}^{(1)} \quad (72)$$

in the initial configuration. Eventually, the mortar integrals on each segment can be written as

$$\begin{aligned} n^{\kappa\beta} &= \int_{\Delta} N^{\kappa}(\boldsymbol{\xi}_{\text{seg}}^{(1),h}(\boldsymbol{\eta})) N^{\beta}(\boldsymbol{\xi}_{\text{seg}}^{(1),h}(\boldsymbol{\eta})) J_{\text{seg}} \, d\boldsymbol{\eta} \\ n^{\kappa\zeta} &= \int_{\Delta} N^{\kappa}(\boldsymbol{\xi}_{\text{seg}}^{(1),h}(\boldsymbol{\eta})) N^{\zeta}(\boldsymbol{\xi}_{\text{seg}}^{(2),h}(\boldsymbol{\eta})) J_{\text{seg}} \, d\boldsymbol{\eta} \end{aligned} \quad (73)$$

The segment contributions to the mortar mesh-tying constraints are collected in the vector

$$\tilde{\boldsymbol{\Phi}}_{e,\text{seg}}(\mathbf{q}, \boldsymbol{\Theta}) = \begin{bmatrix} \tilde{\boldsymbol{\Phi}}_{e,\text{seg}}^{\kappa=1}(\mathbf{q}, \boldsymbol{\Theta}) \\ \vdots \\ \tilde{\boldsymbol{\Phi}}_{e,\text{seg}}^{\kappa=4}(\mathbf{q}, \boldsymbol{\Theta}) \end{bmatrix} \quad (74)$$

where

$$\tilde{\boldsymbol{\Phi}}_{e,\text{seg}}^{\kappa}(\mathbf{q}, \boldsymbol{\Theta}) = \sum_{\beta} n^{\kappa\beta} \begin{bmatrix} \mathbf{q}_{\beta}^{(1)} \\ \boldsymbol{\Theta}_{\beta}^{(1)} \end{bmatrix} - \sum_{\zeta} n^{\kappa\zeta} \begin{bmatrix} \mathbf{q}_{\zeta}^{(2)} \\ \boldsymbol{\Theta}_{\zeta}^{(2)} \end{bmatrix} \quad (75)$$

To perform the assembly of the contributions of all elements $e \in \bar{\mathcal{E}}^{(1)}$ on the non-mortar side, the connection between local and global node numbers is stored in the location array LM, so that $A = \text{LM}(\kappa, e)$, for $A \in \bar{\omega}^{(1)}$, $\kappa \in \{1, \dots, 4\}$ and $e \in \bar{\mathcal{E}}^{(1)}$. Accordingly, the mortar constraints follow from

$$\boldsymbol{\Phi}_{\text{mortar}}^A \leftarrow \boldsymbol{\Phi}_{\text{mortar}}^A + \boldsymbol{\Phi}_e^{\kappa} \quad (76)$$

Or equivalently

$$\boldsymbol{\Phi}_{\text{mortar}}(\mathbf{q}, \boldsymbol{\Theta}) = \mathbf{A} \underset{e \in \bar{\mathcal{E}}^{(1)}}{\tilde{\boldsymbol{\Phi}}_e} = \mathbf{A} \underset{e \in \bar{\mathcal{E}}^{(1)} \text{ seg}}{\cup} \tilde{\boldsymbol{\Phi}}_{e,\text{seg}} = \mathbf{A} \underset{e \in \bar{\mathcal{E}}^{(1)} \text{ seg}}{\cup} \begin{bmatrix} \tilde{\boldsymbol{\Phi}}_{e,\text{seg}}^{\kappa=1}(\mathbf{q}, \boldsymbol{\Theta}) \\ \vdots \\ \tilde{\boldsymbol{\Phi}}_{e,\text{seg}}^{\kappa=4}(\mathbf{q}, \boldsymbol{\Theta}) \end{bmatrix} \quad (77)$$

5.2. Augmentation

The above mesh-tying constraints are only frame indifferent, if they are fulfilled in the reference configuration (see Puso [20]), which would not be the case in general. To remedy this drawback, we reformulate the domain decomposition constraints in terms of invariants being at most quadratic. Based on the developments in Hesch and Betsch [15] we introduce augmented coordinates \mathbf{d}_A , which equal the nodal normal vector of the discrete interface $\Gamma_d^{(1)}$. To determine the value of the augmented coordinates, we have to apply three additional constraints for each vector \mathbf{d}_A

$$\boldsymbol{\Phi}_A^{\text{aug}}(\mathbf{q}, \mathbf{d}) = \begin{bmatrix} \mathbf{d}_A \cdot \mathbf{a}_1 \\ \mathbf{d}_A \cdot \mathbf{a}_2 \\ \frac{1}{2}(\mathbf{d}_A \cdot \mathbf{d}_A - 1) \end{bmatrix} \quad (78)$$

where \mathbf{a}_i are the tangential vectors, evaluated at the placement of the vector \mathbf{d}_A on the interface[‡]. Similar to the above introduction of system vectors \mathbf{q} and Θ we collect the augmented coordinates into a system vector $\mathbf{d} = [\mathbf{d}_1, \dots, \mathbf{d}_{n_{\text{surf}}}]$. In contrast to the use of nodal normal vectors, we have applied in our previous developments [15] a single vector \mathbf{d}_{seg} for each segment. Thus, there are overall six additional unknowns (three additional coordinates and three Lagrange multipliers) for each segment. In the present work, a dramatic decrease of unknowns is achieved by using a single vector \mathbf{d}_κ at each node κ on the mortar side of the interface. Interpolating this vector using standard shape functions of the underlying geometry (cf. Betsch and Sanger [24, Section 3]) yields

$$\mathbf{d}_{\text{seg}} = \sum_{\kappa} N^{\kappa}(\xi_{\text{seg}}^{(1),h}(\boldsymbol{\eta})) \mathbf{d}_{\kappa} \tag{79}$$

To simplify the numerical quadrature of the mortar integrals, we keep \mathbf{d}_{seg} constant within each segment. In particular, we evaluate \mathbf{d}_{seg} at the fourth Gauss point $\boldsymbol{\eta}_{GP_4} = [\frac{1}{3}, \frac{1}{3}]$ (see Figure 2(d)) in the segment, where we also evaluate the tangential vectors

$$\mathbf{a}_{1,\text{seg}} = \sum_{\kappa} N^{\kappa}_{,\xi_i}(\xi_{\text{seg}}^{(1),h}(\boldsymbol{\eta}_{GP_4})) \mathbf{q}_{\kappa} \tag{80}$$

At last, we obtain the following modified constraint functions:

$$\tilde{\Phi}_{e,\text{seg}}^{\kappa}(\mathbf{q}, \Theta, \mathbf{d}) = \begin{bmatrix} \Phi_{e,\text{seg}}^{\kappa}(\mathbf{q}, \Theta) \cdot \begin{bmatrix} \mathbf{a}_{1,\text{seg}} \\ 0 \end{bmatrix} \\ \Phi_{e,\text{seg}}^{\kappa}(\mathbf{q}, \Theta) \cdot \begin{bmatrix} \mathbf{a}_{2,\text{seg}} \\ 0 \end{bmatrix} \\ \Phi_{e,\text{seg}}^{\kappa}(\mathbf{q}, \Theta) \cdot \begin{bmatrix} \mathbf{d}_{\text{seg}} \\ 0 \end{bmatrix} \\ \Phi_{e,\text{seg}}^{\kappa}(\mathbf{q}, \Theta) \cdot \begin{bmatrix} \mathbf{0} \\ 1 \end{bmatrix} \end{bmatrix} \tag{81}$$

Collecting the above segment contributions into a system vector yields

$$\Phi(\mathbf{q}, \Theta, \mathbf{d}) = \begin{bmatrix} \Phi_{A=1}^{\text{aug}}(\mathbf{q}, \mathbf{d}) \\ \vdots \\ \Phi_{A=n_{\text{surf}}}^{\text{aug}}(\mathbf{q}, \mathbf{d}) \\ \Phi_{\text{mortar}}^{A=1}(\mathbf{q}, \Theta, \mathbf{d}) \\ \vdots \\ \Phi_{\text{mortar}}^{A=n_{\text{surf}}}(\mathbf{q}, \Theta, \mathbf{d}) \end{bmatrix} \tag{82}$$

Similarly, the Lagrange multipliers corresponding to the coordinate augmentation and the mortar constraints are collected in the system vector $\boldsymbol{\lambda}$. Overall we obtain seven constraints per node on the mortar side.

5.3. Time discretization

The last step in our development is to discretize the constrained, finite dimensional system in time and to verify the algorithmic conservation properties. Basically we have to discretize a

[‡]Note that the tangential vectors are not uniquely defined at the nodes on a $C^{(0)}$ surface. A common approach is to use an average of the tangential vectors of the adjacent elements.

thermomechanical system subject to holonomic constraints. We refer to previous developments (see Hesch and Betsch [15]) concerning purely mechanical systems in the context of domain decomposition problems and to Betsch & Steinmann [7] and Gonzalez [25] for details concerning the time discretization of holonomic constraints.

As before, we evaluate the primary variables (position, temperature, and augmented coordinates) using a mid-point-type approximation, whereas the Lagrange multipliers $\lambda \rightarrow \lambda_{n,n+1}$ remain constant within each time step

$$\begin{aligned} & \delta \mathbf{q}_A \cdot \left[M^{AB} (\mathbf{v}_{B,n+1} - \mathbf{v}_{B,n}) + \Delta t \int_{\mathcal{B}_0} S_{n,n+1}^{AB} dV \mathbf{q}_{B,n+1/2} \right] \\ & = \Delta t \delta \mathbf{q}_A \cdot [\mathbf{F}_{n+1/2}^{A,\text{ext}} - \nabla_{\mathbf{q}^A} \Phi(\mathbf{q}_{n+1/2}, \Theta_{n+1/2}, \mathbf{d}_{n+1/2}) \cdot \lambda_{n,n+1}] \\ & \delta \Theta_A \left[\Gamma_{n,n+1}^{AB} \Theta_{B,n+1/2} - \Delta t \int_{\mathcal{B}_0} K_{n,n+1}^{AB} dV \Theta_{B,n+1/2} \right] \\ & = \Delta t \delta \Theta_A [\mathcal{Q}_{n,n+1}^{h,A} - \nabla_{\Theta^A} \Phi(\mathbf{q}_{n+1/2}, \Theta_{n+1/2}, \mathbf{d}_{n+1/2}) \cdot \lambda_{n,n+1}] \\ & \nabla_{\mathbf{d}} \Phi(\mathbf{q}_{n+1/2}, \Theta_{n+1/2}, \mathbf{d}_{n+1/2}) \cdot \lambda_{n,n+1} = \mathbf{0} \\ & \Phi(\mathbf{q}_{n+1}, \Theta_{n+1}, \mathbf{d}_{n+1}) = \mathbf{0} \end{aligned} \quad (83)$$

As we do not change the energy-momentum consistent integrator used for the thermoelastic system, we will focus on the additional terms due to the constraints to verify the conservation properties.

5.3.1. *Linear momentum.* Proceeding along the lines of Section 4.1.1, we now obtain

$$\boldsymbol{\mu} \cdot (\mathbf{L}_{n+1} - \mathbf{L}_n) = \Delta t \boldsymbol{\mu} \cdot \sum_{A \in \omega} (\mathbf{F}_{n+1/2}^{A,\text{ext}} - \nabla_{\mathbf{q}^A} \Phi(\mathbf{q}_{n+1/2}, \Theta_{n+1/2}, \mathbf{d}_{n+1/2}) \cdot \lambda_{n,n+1}) \quad (84)$$

Frame-indifference of the vector of constraints Φ has already been shown in detail in Hesch and Betsch [15] for the purely mechanical case. It can be easily verified that

$$\Phi(\mathbf{q}_\varepsilon, \Theta_{n+1/2}, \mathbf{d}_{n+1/2}) = \Phi(\mathbf{q}_{n+1/2}, \Theta_{n+1/2}, \mathbf{d}_{n+1/2}) \quad (85)$$

Here, $\mathbf{q}_\varepsilon^A = \mathbf{q}_{n+1/2}^A + \varepsilon \boldsymbol{\mu}$, $\forall A \in \omega$ and $\varepsilon \in \mathbb{R}$ is arbitrary. Equation (85) implies

$$\left. \frac{d}{d\varepsilon} \right|_{\varepsilon=0} \Phi(\mathbf{q}_\varepsilon, \Theta_{n+1/2}, \mathbf{d}_{n+1/2}) = \sum_{A \in \omega} [\nabla_{\mathbf{q}^A} \Phi(\mathbf{q}_{n+1/2}, \Theta_{n+1/2}, \mathbf{d}_{n+1/2}) \boldsymbol{\mu}] \cdot \boldsymbol{\mu} = 0 \quad (86)$$

Insertion in (84) yields

$$\mathbf{L}_{n+1} - \mathbf{L}_n = \Delta t \sum_{A \in \omega} \mathbf{F}_{n+1/2}^{A,\text{ext}} \quad (87)$$

which confirms that the constraints do not affect linear momentum conservation.

5.3.2. *Angular momentum.* Proceeding along the lines of Section 4.1.2, (53) is replaced by

$$\boldsymbol{\mu} \cdot (\mathbf{J}_{n+1} - \mathbf{J}_n) = \Delta t \boldsymbol{\mu} \cdot \left(\sum_{A \in \omega} \mathbf{q}_{A,n+1/2} \times [\mathbf{F}_{n+1/2}^{A,\text{ext}} - \nabla_{\mathbf{q}^A} \Phi(\mathbf{q}_{n+1/2}, \Theta_{n+1/2}, \mathbf{d}_{n+1/2}) \cdot \lambda_{n,n+1}] \right) \quad (88)$$

Based on the results in Hesch and Betsch [15] we can postulate for the domain decomposition constraints

$$\Phi(\mathbf{q}_\varepsilon, \Theta_{n+1/2}, \mathbf{d}_{n+1/2}) = \Phi(\mathbf{q}_{n+1/2}, \Theta_{n+1/2}, \mathbf{d}_\varepsilon) \quad (89)$$

where $\mathbf{q}_\varepsilon^A = \exp(\varepsilon \hat{\boldsymbol{\mu}}) \mathbf{q}_{n+1/2}^A, \forall A \in \omega$ and $\mathbf{d}_\varepsilon^A = \exp(-\varepsilon \hat{\boldsymbol{\mu}}) \mathbf{d}_{n+1/2}^A, \forall A \in \bar{\omega}^{(1)}$. Accordingly, we can write in analogy to (86)

$$\begin{aligned} \left. \frac{d}{d\varepsilon} \right|_{\varepsilon=0} [\Phi(\mathbf{q}_\varepsilon, \Theta_{n+1/2}, \mathbf{d}_{n+1/2}) - \Phi(\mathbf{q}_{n+1/2}, \Theta_{n+1/2}, \mathbf{d}_\varepsilon)] &= 0 \\ \sum_{A \in \omega} [\nabla_{\mathbf{q}^A} \Phi(\mathbf{q}_{n+1/2}, \Theta_{n+1/2}, \mathbf{d}_{n+1/2}) \cdot (\boldsymbol{\mu} \times \mathbf{q}_{n+1/2}^A) & \\ - \nabla_{\mathbf{d}^A} \Phi(\mathbf{q}_{n+1/2}, \Theta_{n+1/2}, \mathbf{d}_{n+1/2}) \cdot (\boldsymbol{\mu} \times \mathbf{d}_{n+1/2}^A)] &= 0 \end{aligned} \tag{90}$$

Due to (83)₃ the last term in the square brackets of (90)₂ vanishes. Inserting the last equation into (88) yields

$$\mathbf{J}_{n+1} - \mathbf{J}_n = \Delta t \sum_{A \in \omega} \mathbf{q}_{A,n+1/2} \times \mathbf{F}_{n+1/2}^{A,\text{ext}} \tag{91}$$

which confirms that the constraints do not affect angular momentum conservation as well.

5.3.3. *Total energy.* Eventually, we verify algorithmic energy consistency. Proceeding along the lines of Section 4.1.3, we can restrict ourselves to the contributions of the constraints. In particular, we have to show that these contributions are workless. For the mechanical part, conservation of energy can be proven following the arguments in Hesch and Betsch [15, Section 6.1]. Similar to result (58), in the present case we obtain

$$T_{n+1} - T_n + E_{n+1} - E_n = \Delta t \left[P_{n,n+1}^{\text{h,ext}} + Q_{n,n+1}^{\text{h}} - \sum_{A \in \omega} \nabla_{\Theta^A} \Phi(\mathbf{q}_{n+1/2}, \Theta_{n+1/2}, \mathbf{d}_{n+1/2}) \cdot \boldsymbol{\lambda}_{n,n+1} \right] \tag{92}$$

With regard to (63) and (62) we can rewrite the last term in the square brackets (92)

$$\sum_{B \in \bar{\omega}} (\lambda_A^4)_{n,n+1} n^{AB} - \sum_{C \in \bar{\omega}} (\lambda_A^4)_{n,n+1} n^{AC} = (\lambda_A^4)_{n,n+1} \left(\int_{\Gamma_d^{(1)}} N^A(\mathbf{X}^{(1)}) d\Gamma - \int_{\Gamma_d^{(1)}} N^A(\mathbf{X}^{(1)}) d\Gamma \right) = 0 \tag{93}$$

where we have made use of the property $\sum_B N^B(\mathbf{X}^{(1)}) = 1$. Taking into account the last result, (92) yields

$$T_{n+1} - T_n + E_{n+1} - E_n = \Delta t [P_{n,n+1}^{\text{h,ext}} + Q_{n,n+1}^{\text{h}}] \tag{94}$$

which confirm that the constraints are workless.

Remark

The last statement depends crucially on the accuracy of the numerical evaluation of the mortar integrals for each segment. Remarkably, the proof for linear momentum conservation in Puso [20] leads to the same conclusion. Our numerical experiments have shown that a four point Gauss integration is sufficient.

6. EXAMPLES

In this section we evaluate the accuracy and performance of the newly proposed method. An incremental iterative Newton–Raphson solution procedure has been implemented in MATLAB to solve monolithically the non-linear system of equations (48) or (84). The data for the used Ogden model are similar to Holzapfel and Simo [4] and are summarized in Table I (see Appendix A for a summary of the constitutive equations). Enhanced assumed strain elements (see Appendix B for details) have been implemented as well. For all examples we define a stress free reference state in thermal equilibrium based on a homogeneous temperature field $\Theta_0 = 293.15 \text{ K}$.

Table I. Material properties.

Ogden model	$\mu_1 = 6.30 \times 10^5 \text{ N/m}^2$ $\mu_2 = 0.012 \times 10^5 \text{ N/m}^2$ $\mu_3 = -0.10 \times 10^5 \text{ N/m}^2$	$\alpha_1 = 1.3$ $\alpha_2 = 5.0$ $\alpha_3 = -2.0$
Heat capacity	$c_0 = 1830 \text{ Nm/kgK}$	
Density	$\rho_0 = 950 \text{ kg/m}^3$	
Linear expansion coefficient	$\alpha_0 = 22.333 \times 10^{-5} \text{ K}^{-1}$	
Bulk modulus	$\kappa(\Theta_0) = 2.0 \times 10^8 \text{ N/m}^2$	
Empirical coefficients	$\beta = 9.0$ $\gamma = 2.50$	
Thermal conductivity	$K_0(\Theta_0) = 0.15 \text{ N/sK}$	
Softening parameter	$\omega_K = 0.004$	

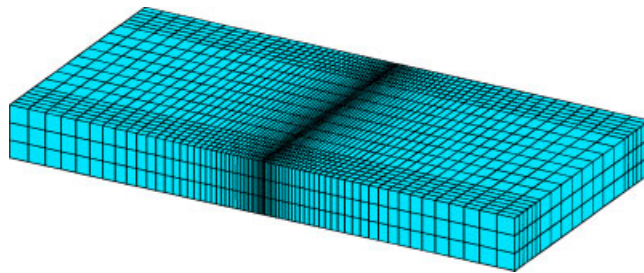


Figure 3. Reference configuration.

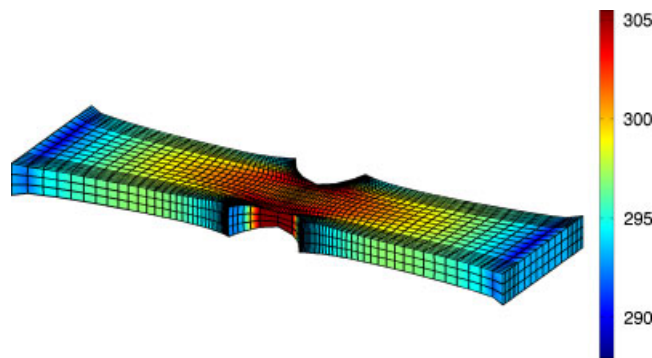


Figure 4. Deformed configuration of the cracked rectangular bar. The temperature distribution is color coded.

6.1. Three-dimensional cracked rectangular bar

As a first example we consider a quasi-static system by setting the density artificially to zero. Apart from that, the coupled transient system has been calculated. Based on the last example in Holzapfel and Simo [4] we define a rectangular bar of the size $10\text{ m} \times 4.8\text{ m} \times 1\text{ m}$. A crack of $1/3$ of the width has been inserted into the middle of the system. The reference mesh is displayed in Figure 3.

The mesh consists of 6912 elements with 36 740 thermal and mechanical degrees of freedom. Furthermore, 62 208 enhanced strain modes are used. Both sides are clamped, i.e. Dirichlet boundary conditions have been applied to the mechanical as well as the thermal boundary, keeping the temperature constant on the boundary at $\Theta_0 = 293.15 \text{ K}$. Within each time step $\Delta t = 1 \text{ s}$ both sides are moved apart with $\Delta x = 0.02 \text{ m}$, until an increase of the length of 65% has been reached. The resulting temperature distribution is displayed in Figure 4. As can be seen, the Dirichlet

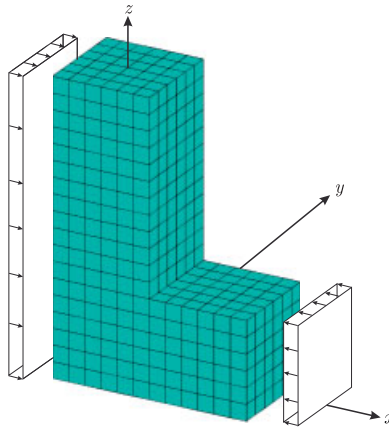


Figure 5. Pressure load on boundaries.

boundaries on both sides are fulfilled exactly. As expected, we receive the highest changes in temperature at the crack tip.

6.2. Thermoelastic problem

The next problem under consideration consists of a three-dimensional L -shaped block of the size $2.4\text{ m} \times 3.6\text{ m} \times 1.2\text{ m}$. The L -shape has been discretized with 864 elements leading to overall 4900 mechanical and thermal degrees of freedom. We apply a sinusoidal pressure load $p_{\max} = 25\,000\text{ N/m}^2$ during the time interval $t \in [0, 1]$ to the outer surfaces, as shown in Figure 5. No thermal boundary conditions have been set, hence the system is adiabatically isolated after the load phase. Thus, the body moves freely in space for $t \in [1, 5]$. Due to the initial loading conditions, the body rotates about three times around the y -axis within 5 s.

Three different simulations have been performed:

- *Integrator 1*: Newly developed energy-momentum consistent scheme (48) or (84).
- *Integrator 2*: Standard mid-point rule, however the right Cauchy-Green tensor has been evaluated according to (26).
- *Integrator 3*: Standard mid-point rule.

All three integrators conserve linear and angular momentum. For the proposed energy-momentum scheme the fulfillment of the discrete balance of angular momentum (cf. (53) and (91)) is confirmed in Figure 7. A time step size of $\Delta t = 0.01\text{ s}$ has been used during the load phase. After the load phase, the time step size has been doubled to $\Delta t = 0.02\text{ s}$ for integrators 1 and 2, whereas for the integrator 3 the time step size has been changed to $\Delta t = 0.011\text{ s}$ (larger time steps for the integrator 3 are not possible).

In Figure 6 the absolute values of change in total energy (i.e. the total mechanical and the thermal energy) in each time step after the end of the load phase are plotted in a semilogarithmic scale.

As expected, the change in total energy for the energy-momentum scheme is below the stop criterion of the Newton iterations for which the value 10^{-5} for the norm of the residual vector has been prescribed. Without the concept of the discrete gradient, total energy will not be conserved, but as the results clearly show the simulation remains stable using the integrator 2. The third integrator diverges 19 time steps after the end of the load phase.

6.3. Convergence analysis

To evaluate the accuracy of the proposed algorithm, we simplify the thermoelastic problem in Section 6.2. Four elements are used to discretize the L -Shape, furthermore the maximum pressure has been changed to $p_{\max} = 65\,000\text{ N/m}^2$ and applied for the first 0.5 s as shown in Figure 8.

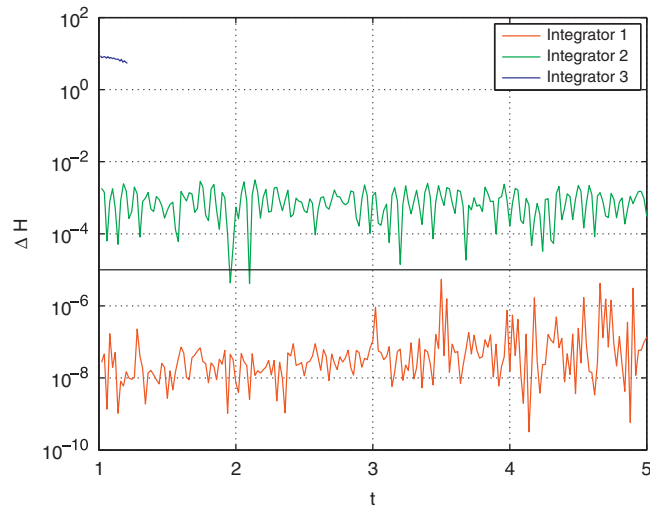


Figure 6. Change in total energy within each time step.

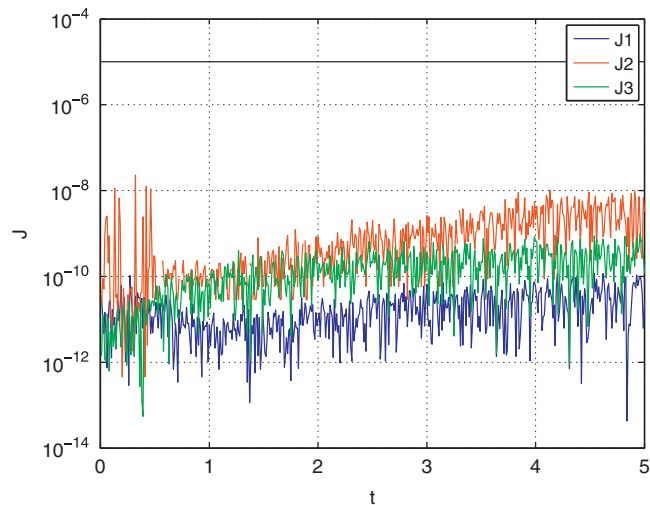


Figure 7. Change in angular momentum within each time step.

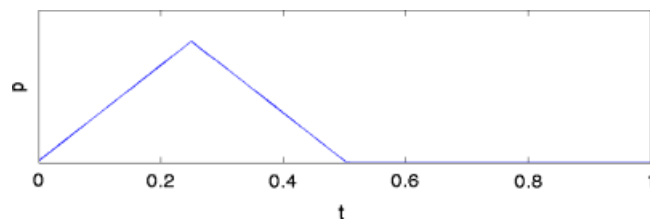


Figure 8. Load curve for the convergence analysis.

Additionally, we changed the Bulk modulus to $\kappa(\Theta_0) = 2.0 \times 10^5 \text{ N/m}^2$, such that the body can change its volume. The maximum temperature reached $\Theta_{\max} \approx 296 \text{ K}$ and the minimum temperature $\Theta_{\min} \approx 291 \text{ K}$. After the load phase, the calculation was terminated at $t = 1 \text{ s}$. We calculate a reference solution \mathbf{q}_{Ref} using a time step size of $\Delta t = 10^{-4} \text{ s}$. Note that we set the tolerance of the Newton iteration to 10^{-6} with regard to the L_2 -norm of the residual vector for all calculations. To run

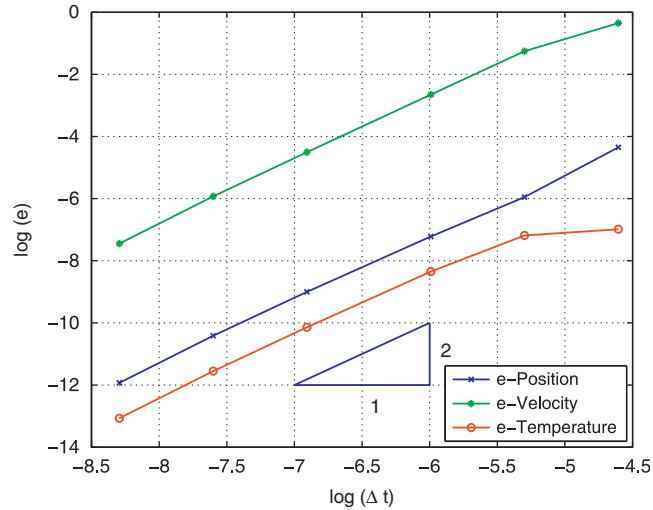


Figure 9. Convergence results.

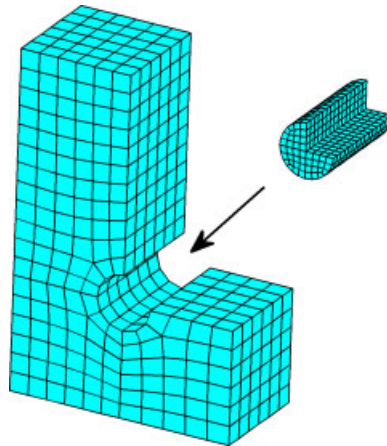


Figure 10. Reference configuration.

the analysis, we have calculated the system using $\Delta t \in \{10^{-2} \text{ s}, 5 \times 10^{-3} \text{ s}, 2.5 \times 10^{-3} \text{ s}, 10^{-3} \text{ s}, 5 \times 10^{-4} \text{ s}, 2.5 \times 10^{-4} \text{ s}\}$. The relative error for the discrete system has been determined as follows:

$$e_q = \sum_{A=1}^{n_{\text{node}}} \frac{\|\mathbf{q}_A - \mathbf{q}_{A,\text{Ref}}\|}{\|\mathbf{q}_{A,\text{Ref}}\|} \quad (95)$$

The values for the velocity as well as for the temperature have been generated analogously. As can be observed from Figure 9, the proposed algorithm is second-order accurate.

6.4. Thermal domain decomposition problem

This example utilizes the same geometry of a three-dimensional *L*-shape as before. However, two subdomains of the *L*-shaped block have been meshed independently (see Figure 10). The larger subdomain consists of 840 elements, whereas the smaller subdomain consists of 675 elements. 1584 segments have to be computed for the domain decomposition interface. Additional 77 normal vectors with altogether 231 augmented coordinates as unknowns are used. In contrast to the present node-based augmentation, our original segment-based augmentation technique (see Hesch and Betsch [15]) leads to 1584 normal vectors with altogether 4785 additional unknowns.

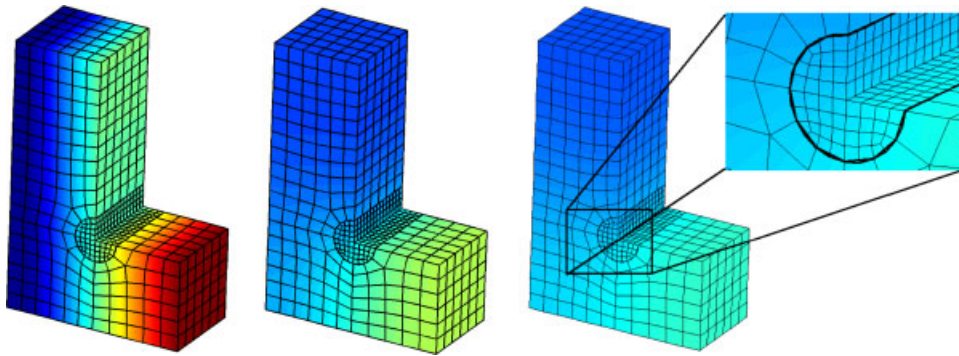


Figure 11. Temperature distribution at different times.

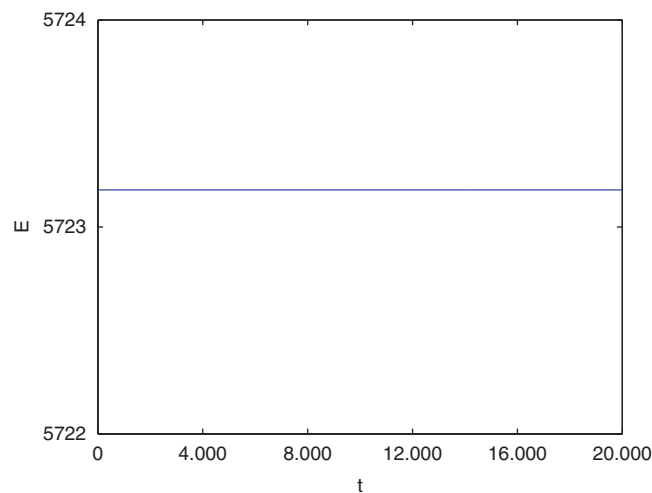


Figure 12. Energy over time (in s).

Thus, the system consists of overall 9110 thermal, mechanical, and augmented degrees of freedom in conjunction with 539 constraints (231 constraints for the augmented coordinates and 308 for the mortar constraints). First we examine the influence of the mortar method on the pure heat conduction problem, i.e. we exclude all mechanical equations from the system and apply a linear distribution of temperature to the adiabatically isolated L-shape (cf. Figure 11, left). Figure 11 (central) shows the temperature distribution after 2 h 45 min, whereas Figure 11 (right) shows the temperature distribution after 5 h 30 min. At this time, thermodynamic equilibrium has nearly been reached. Figure 12 shows the total energy of the system over time.

As can be seen, energy is conserved, which reflects the first law of thermodynamics. The second law states that the entropy production remains equal or greater zero, which can be observed in this particular example from Figure 13.

6.5. Thermoelastic domain decomposition problem

We next deal with the completely coupled, transient thermoelastic problem. The same mechanical configuration as in Example 6.4 has been used combined with the load phase described in Example 6.2. Again, after the load phase the adiabatically isolated system moves freely in space and the time step size has been set to $\Delta t = 0.02$ s. The proposed energy-momentum consistent scheme obeys the first law of thermodynamics, as shown in Figure 14. For the problem at hand, the entropy production is displayed in Figure 15.

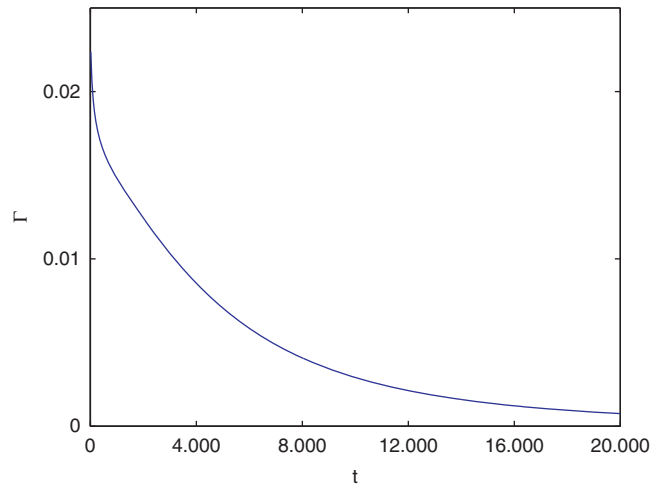


Figure 13. Entropy production over time (in s).

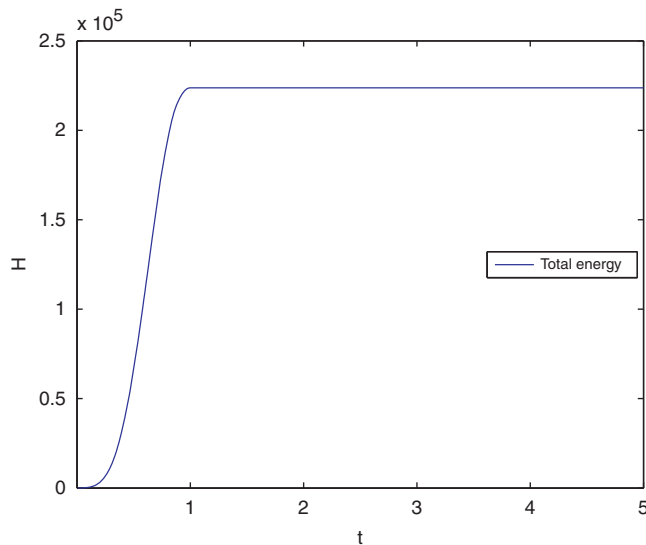


Figure 14. Energy over time (in s).

7. CONCLUSIONS

A novel energy-momentum consistent scheme for thermoelastodynamics along with its extension to domain decomposition problems has been presented. The present approach can be viewed as straightforward extension of energy-momentum integrators to the realm of thermoelasticity. In essence, the present method relies on an enhancement of the notion of a discrete gradient to the coupled problem at hand. Arbitrary constitutive laws for thermoelasticity can be directly used. This is in contrast to the design of thermodynamically consistent integrators proposed by Romero [11, 12], which requires a reformulation within the GENERIC framework.

The extension of the present energy-momentum consistent approach to domain decomposition problems is based on a four-dimensional mortar method for thermoelastic systems. Our new developments imply a significant modification of our original approach which has been confined to isothermal problems. In particular the present work reduces the number of augmented unknowns as well as the number of constraints drastically, improving the performance of the mortar method far beyond the performance of previous approaches.

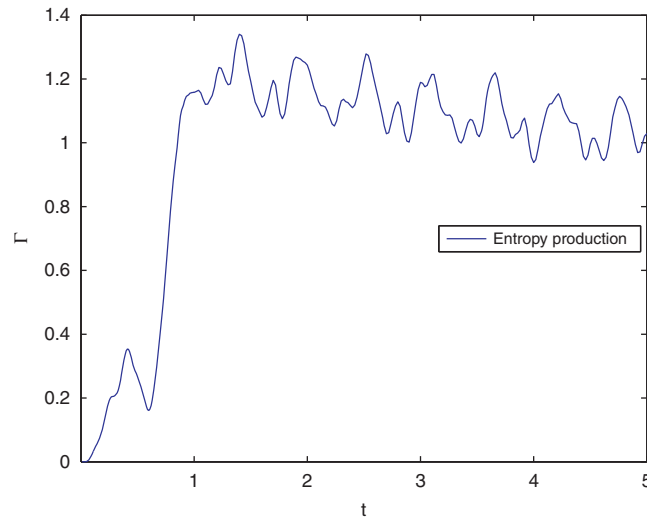


Figure 15. Entropy production over time (in s).

The present work will provide the foundation for the development of new energy-momentum consistent integrators for thermomechanically coupled contact problems. Mortar-based algorithms for large deformation contact will be the subject of a follow-up paper.

APPENDIX A: CONSTITUTIVE EQUATIONS

The constitutive equations rely on the developments of Holzapfel and Simo [4], where a detailed derivation of the equations can be found. Since the development of constitutive equations is not the main focus of this paper, we restrict ourselves to the well-known Ogden material given in the aforementioned paper, written in terms of the eigenvalues λ_A^2 , $A \in [1, 2, 3]$ of the right Cauchy-Green tensor.

A.1. Free Helmholtz energy

Since materials like rubber behave differently in bulk and shear, we split the free Helmholtz energy function additive into a volumetric and deviatoric part

$$\Psi = \hat{\Psi}(\lambda_1, \lambda_2, \lambda_3, \theta) = \hat{U}(J, \theta) + \sum_{A=1}^3 \tilde{\Psi}(\tilde{\lambda}_A, \theta) \quad (\text{A1})$$

with $J = \lambda_1 \lambda_2 \lambda_3$ and $\tilde{\lambda}_A = J^{-1/3} \lambda_A$. The volumetric part reads as

$$\hat{U}(J, \theta) = \kappa(\theta) G(J) - \frac{e_0}{\theta_0} (\theta - \theta_0) + \hat{T}(\theta) \quad (\text{A2})$$

with

$$\begin{aligned} \kappa(\theta) &= \kappa(\theta_0) \frac{\theta}{\theta_0} \\ G(J) &= \beta^{-2} [\beta \ln(J) + J^{-\beta} - 1] \\ \frac{e_0}{\theta_0} (\theta - \theta_0) &= 3\alpha_0 \kappa(\theta_0) \gamma^{-1} (J^\gamma - 1) (\theta - \theta_0) \\ \hat{T}(\theta) &= c_0 \left[\theta - \theta_0 - \theta \ln \left(\frac{\theta}{\theta_0} \right) \right] \end{aligned} \quad (\text{A3})$$

On the other hand, the deviatoric part reads as

$$\tilde{\Psi}(\tilde{\lambda}_A, \theta) = \sum_{p=1}^N \frac{\mu_p(\theta_0) \frac{\theta}{\theta_0}}{\alpha_p} (\tilde{\lambda}_A^{\alpha_p} - 1) \tag{A4}$$

A.2. Derivatives of the free Helmholtz energy

With regard to the additive split of the free Helmholtz energy (A1), we can split the second Piola-Kirchhoff stress tensor as

$$\Sigma = \Sigma_{\text{vol}} + \Sigma_{\text{iso}} \tag{A5}$$

The volumetric part of the stress tensor reads as

$$\Sigma_{\text{vol}} = 2 \frac{\partial \hat{\Psi}_{\text{vol}}(J, \theta)}{\partial \mathbf{C}} = \frac{\partial \hat{\Psi}_{\text{vol}}(J, \theta)}{\partial J} J \mathbf{C}^{-1} \tag{A6}$$

with

$$\frac{\partial \hat{\Psi}_{\text{vol}}(J, \theta)}{\partial J} J = \kappa(\theta_0) \frac{\theta}{\theta_0} \beta^{-1} [1 - J^{-\beta}] - 3\alpha_0 \kappa(\theta_0) J^\gamma (\theta - \theta_0) \tag{A7}$$

For the derivatives of $\hat{\Psi}_{\text{iso}}$ we recall the relation

$$\begin{aligned} \frac{\partial \tilde{\lambda}_A}{\partial \lambda_B} &= \frac{\partial (J^{-1/3} \lambda_A)}{\partial \lambda_B} = J^{-1/3} \delta_{AB} + \frac{\partial J^{-1/3}}{\partial \lambda_B} \lambda_A \\ &= J^{-1/3} \delta_{AB} - \frac{1}{3} J^{-4/3} \frac{\partial J}{\partial \lambda_B} \lambda_A = J^{-1/3} \left(\delta_{AB} - \frac{1}{3} \lambda_A \lambda_B^{-1} \right) \end{aligned} \tag{A8}$$

The isochoric contribution to the stress tensor reads as

$$\Sigma_{\text{iso}} = 2 \frac{\partial \hat{\Psi}_{\text{iso}}(\tilde{\lambda}_1, \tilde{\lambda}_2, \tilde{\lambda}_3, \theta)}{\partial \mathbf{C}} = \sum_{A=1}^3 \frac{1}{\lambda_A} \frac{\partial \hat{\Psi}_{\text{iso}}}{\partial \lambda_A} \hat{N}_A \otimes \hat{N}_A \tag{A9}$$

with

$$\begin{aligned} \frac{\partial \hat{\Psi}_{\text{iso}}}{\partial \lambda_A} &= \frac{\partial \hat{\Psi}_{\text{iso}}}{\partial \tilde{\lambda}_B} \frac{\partial \tilde{\lambda}_B}{\partial \lambda_A} = J^{-1/3} \left(\frac{\partial \hat{\Psi}_{\text{iso}}}{\partial \tilde{\lambda}_A} - \frac{1}{3} \sum_{B=1}^3 \frac{\lambda_B}{\lambda_A} \frac{\partial \hat{\Psi}_{\text{iso}}}{\partial \tilde{\lambda}_B} \right) \\ &= \frac{1}{\lambda_A} \left(\tilde{\lambda}_A \frac{\partial \hat{\Psi}_{\text{iso}}}{\partial \tilde{\lambda}_A} - \frac{1}{3} \sum_{B=1}^3 \tilde{\lambda}_B \frac{\partial \hat{\Psi}_{\text{iso}}}{\partial \tilde{\lambda}_B} \right) \end{aligned} \tag{A10}$$

and

$$\frac{\partial \hat{\Psi}_{\text{iso}}}{\partial \tilde{\lambda}_A} = \sum_{p=1}^N \mu_p(\theta_0) \frac{\theta}{\theta_0} \tilde{\lambda}_A^{\alpha_p - 1} \tag{A11}$$

Thus, we obtain

$$2 \frac{\partial \hat{\Psi}_{\text{iso}}(\lambda_1, \lambda_2, \lambda_3, \theta)}{\partial \mathbf{C}} = \sum_{A=1}^3 \left\{ \frac{1}{\lambda_A^2} \left[\sum_{p=1}^N \mu_p(\theta_0) \frac{\theta}{\theta_0} \tilde{\lambda}_A^{\alpha_p} - \frac{1}{3} \sum_{B=1}^3 \sum_{p=1}^N \mu_p(\theta_0) \frac{\theta}{\theta_0} \tilde{\lambda}_B^{\alpha_p} \right] \hat{N}_A \otimes \hat{N}_A \right\} \tag{A12}$$

For the sake of completeness we deduce the derivative of the free Helmholtz energy function with respect to the temperature

$$\begin{aligned} \frac{\partial \hat{\Psi}_{\text{iso}}(\lambda_1, \lambda_2, \lambda_3, \theta)}{\partial \theta} &= \frac{\kappa(\theta_0)}{\theta_0 \beta^2} [\beta \ln(J) + J^{-\beta} - 1] - 3\alpha_0 \kappa(\theta_0) \gamma^{-1} (J^\gamma - 1) \\ &\quad - c_0 \ln\left(\frac{\theta}{\theta_0}\right) + \sum_{A=1}^3 \sum_{p=1}^N \frac{\mu_p(\theta_0)}{\theta_0 \alpha_p} (\tilde{\lambda}_A^{\alpha_p} - 1) \\ &= -\eta \end{aligned} \quad (\text{A13})$$

A.3. Duhamel's law

Concerning the thermal conductivity tensor in (2) we set

$$\hat{\mathbf{K}}(\mathbf{C}, \theta) = K_0(\theta) \mathbf{C}^{-1} \quad (\text{A14})$$

with

$$K_0(\theta) = K_0(\theta_0) [1 - w_K(\theta - \theta_0)] \quad (\text{A15})$$

Note that the above constitutive laws are in accordance with the second law of thermodynamics.

APPENDIX B: ENHANCED ASSUMED STRAIN METHOD

Standard displacement-based elements are subject to volumetric locking effects in the incompressible limit. To enhance the performance of the tri-linear displacement elements we incorporate the enhanced assumed strain method developed by Simo *et al.* [26, 27] into the present energy-momentum consistent framework.

Based on the developments in Simo *et al.* [27] the following operator is introduced:

$$\widetilde{\text{Grad}}_X(\bullet) = \frac{j_0}{j(\xi)} \mathbf{J}_0^{-T} \text{Grad}_\xi(\bullet) \quad (\text{B1})$$

with

$$\mathbf{J}(\xi) = \frac{\partial \mathbf{X}^h}{\partial \xi}, \quad \mathbf{J}_0 = \mathbf{J}(\xi) \Big|_{\xi=0}, \quad j(\xi) = \det[\mathbf{J}(\xi)], \quad j_0 = j(\mathbf{0}) \quad (\text{B2})$$

The enhanced deformation gradient can now be written as

$$\mathbf{F}^h = \sum_{A=1}^{n_{\text{node}}} \mathbf{q}_A \otimes \widehat{\text{Grad}}_X(N^A) + \sum_{A=1}^{n_{\text{enh}}} \boldsymbol{\alpha}_A \otimes \widetilde{\text{Grad}}_X(M^A) \quad (\text{B3})$$

where

$$\widehat{\text{Grad}}(N^A) = \text{Grad}_0(N^A) + \sum_{J=1}^4 \gamma_J^A \widetilde{\text{Grad}}_X(\mathcal{H}^J) \quad (\text{B4})$$

Here, γ_J are gamma-stabilization vectors and \mathcal{H}^J hourglass functions, defined in Belytschko *et al.* [28]. Additionally we introduce Wilson's incompatible shape functions (see Wilson *et al.* [29]) for tri-linear brick elements

$$\mathbf{M}^1 = \frac{1}{2}[\xi_1^2 - 1], \quad \mathbf{M}^2 = \frac{1}{2}[\xi_2^2 - 1], \quad \mathbf{M}^3 = \frac{1}{2}[\xi_3^2 - 1] \quad (\text{B5})$$

Now the discrete enhanced version of (10)₁ reads as

$$\int_{\mathcal{B}_0} \delta \boldsymbol{\varphi}^h \cdot \dot{\boldsymbol{\pi}}^h + \mathbf{F}^h \boldsymbol{\Sigma}^h : \widehat{\text{Grad}}(\delta \boldsymbol{\varphi}^h) dV = \int_{\partial \mathcal{B}_0^T} \delta \boldsymbol{\varphi}^h \cdot \bar{\mathbf{T}} dA + \int_{\mathcal{B}_0} \delta \boldsymbol{\varphi}^h \cdot \bar{\mathbf{B}} dV \quad (\text{B6})$$

$$\int_{\mathcal{B}_0} \mathbf{F}^h \boldsymbol{\Sigma}^h : \widetilde{\text{Grad}}(\delta \boldsymbol{\alpha}^h) dV = \mathbf{0}$$

where $\boldsymbol{\alpha}^h = \sum_{A=1}^{n_{\text{enh}}} M^A \boldsymbol{\alpha}_A$. Concerning the discretization in time the additional $\boldsymbol{\alpha}$ -modes are evaluated in the mid-point

$$\boldsymbol{\alpha}_{n+1/2}^h = \frac{1}{2}(\boldsymbol{\alpha}_n^h + \boldsymbol{\alpha}_{n+1}^h) \quad (\text{B7})$$

The enhanced form of the fully discrete system (48) can now be written in the form

$$\delta \mathbf{q}_A \cdot \left[M^{AB}(\mathbf{v}_{B,n+1} - \mathbf{v}_{B,n}) + \Delta t \int_{\mathcal{B}_0} \widehat{\text{Grad}}(N^B) \cdot \boldsymbol{\Sigma}_{n,n+1}^h \mathbf{F}_{n+1/2}^h dV \right] = \Delta t \delta \mathbf{q}_A \cdot [\mathbf{F}_{n+1/2}^{A,\text{ext}}]$$

$$\delta \boldsymbol{\alpha} \cdot \left[\int_{\mathcal{B}_0} \widetilde{\text{Grad}}_X(M^A) \cdot \boldsymbol{\Sigma}_{n,n+1}^h \mathbf{F}_{n+1/2}^h dV \right] = \mathbf{0} \quad (\text{B8})$$

$$\delta \Theta_A \left[\Gamma_{n,n+1}^{AB} \Theta_{B,n+1/2} - \Delta t \int_{\mathcal{B}_0} K_{n,n+1}^{AB} dV \Theta_{B,n+1/2} \right] = \Delta t \delta \Theta_A Q_{n,n+1}^{h,A}$$

Note that the additional equations (118)₂ can be eliminated using standard condensation procedures. We further remark that the enhancement of the space discretization outlined above does not affect the conservation and consistency properties of the present energy-momentum integrator.

ACKNOWLEDGEMENTS

Support for this research was provided by the Deutsche Forschungsgemeinschaft (DFG) under grant HE 5943/1-1. This support is gratefully acknowledged.

REFERENCES

1. Reese S, Govindjee S. Theoretical and numerical aspects in the thermo-viscoelastic material behaviour of rubber-like polymers. *Mechanics of Time-Dependent Materials* 1998; **1**:357–396.
2. Miehe C. Entropic thermoelasticity at finite strains. Aspects of the formulation and numerical implementation. *Computer Methods in Applied Mechanics and Engineering* 1995; **120**:243–269.
3. Simo JC. Nonlinear stability of the time-discrete variational problem of evolution in nonlinear heat conduction, plasticity and viscoplasticity. *Computer Methods in Applied Mechanics and Engineering* 1990; **88**:111–131.
4. Holzapfel GA, Simo JC. Entropy elasticity of isotropic rubber-like solids at finite strains. *Computer Methods in Applied Mechanics and Engineering* 1996; **132**:17–44.
5. Gonzalez O. Exact energy and momentum conserving algorithms for general models in nonlinear elasticity. *Computer Methods in Applied Mechanics and Engineering* 2000; **190**:1763–1783.
6. Betsch P, Steinmann P. Conserving properties of a time FE method—Part II: time-stepping schemes for non-linear elastodynamics. *International Journal for Numerical Methods in Engineering* 2001; **50**:1931–1955.
7. Betsch P, Steinmann P. Conservation properties of a time FE method—Part III: mechanical systems with holonomic constraints. *International Journal for Numerical Methods in Engineering* 2002; **53**:2271–2304.
8. Hauret P, Le Tallec P. Energy-controlling time integration methods for nonlinear elastodynamics and low-velocity impact. *Computer Methods in Applied Mechanics and Engineering* 2006; **195**:4890–4916.
9. Betsch P, Hesch C. Energy-momentum conserving schemes for frictionless dynamic contact problems. Part I: NTS method. In *IUTAM Symposium on Computational Methods in Contact Mechanics*, IUTAM Book Series, Wriggers P, Nackenhorst U (eds), vol. 3. Springer: Berlin, 2007; 77–96.
10. Hesch C, Betsch P. A mortar method for energy-momentum conserving schemes in frictionless dynamic contact problems. *International Journal for Numerical Methods in Engineering* 2009; **77**:1468–1500.
11. Romero I. Thermodynamically consistent time-stepping algorithms for non-linear thermomechanical systems. *International Journal for Numerical Methods in Engineering* 2009; **79**:706–732.
12. Romero I. Algorithms for coupled problems that preserve symmetries and the laws of thermodynamics—Part I: monolithic integrators and their application to finite strain thermoelasticity. *Computer Methods in Applied Mechanics and Engineering* 2010; **199**:1841–1858.

13. Gross M. Higher-order accurate and energy-momentum consistent discretisation of dynamic finite deformation thermo-viscoelasticity. University of Siegen, urn:nbn:de:hbz:467-3890, 2009.
14. Gonzalez O. Time integration and discrete hamiltonian systems. *Journal of Nonlinear Science* 1996; **6**:449–467.
15. Hesch C, Betsch P. Transient 3d domain decomposition problems: frame-indifferent mortar constraints and conserving integration. *International Journal for Numerical Methods in Engineering* 2010; **82**:329–358.
16. Bernardi C, Maday Y, Patera AT. Domain decomposition by the mortar method. In *Asymptotic and Numerical Methods for Partial Differential Equations with Critical Parameters*, Kaper HG, Garbey M, Pieper GW (eds). Kluwer Academic Publishers: Dordrecht, The Netherlands, 1993; 269–286.
17. Bernardi C, Maday Y, Patera AT. A new nonconforming approach to domain decomposition: the mortar element method. In *Nonlinear Partial Differential Equations and their Applications*, Brezis H, Lions J-L (eds). Longman Scientific & Technical: Harlow, U.K., 1994; 13–51.
18. Krause R, Wohlmuth BI. Nonconforming domain decomposition techniques for linear elasticity. *East West Journal of Numerical Mathematics* 2000; **8**(3):177–206.
19. Dohrmann CR, Key SW, Heinstein MW. Methods for connecting dissimilar three-dimensional finite element meshes. *International Journal for Numerical Methods in Engineering* 2000; **47**:1057–1080.
20. Puso MA. A 3d mortar method for solid mechanics. *International Journal for Numerical Methods in Engineering* 2004; **59**:315–336.
21. Hüeber S, Wohlmuth BI. Thermo-mechanical contact problems on non-matching meshes. *Computer Methods in Applied Mechanics and Engineering* 2009; **198**:1338–1350.
22. Holzapfel GA. *Nonlinear Solid Mechanics*. Wiley: New York, 2001.
23. Gonzalez O, Stuart AM. *A First Course in Continuum Mechanics* (1st edn). Cambridge University Press: Cambridge, 2008.
24. Betsch P, Sanger N. On the use of geometrically exact shells in a conserving framework for flexible multibody dynamics. *Computer Methods in Applied Mechanics and Engineering* 2009; **198**:1609–1630.
25. Gonzalez O. Mechanical systems subject to holonomic constraints: differential algebraic formulations and conservative integration. *Physica D* 1999; **132**:165–174.
26. Simo JC, Armero F. Geometrically non-linear enhanced strain mixed methods and the method of incompatible modes. *International Journal for Numerical Methods in Engineering* 1992; **33**:1413–1449.
27. Simo JC, Armero F, Taylor RL. Improved versions of assumed enhanced strain tri-linear elements for 3D finite deformation problems. *Computer Methods in Applied Mechanics and Engineering* 1993; **110**:359–386.
28. Belytschko T, Ong JS, Liu WK, Kennedy JM. Hourglass control in linear and nonlinear problems. *Computer Methods in Applied Mechanics and Engineering* 1984; **43**:251–276.
29. Wilson EL, Taylor RL, Doherty WP, Ghaboussi J. Incompatible displacement models. *Numerical and Computer Models in Structural Mechanics*. Academic Press: New York, 1973.